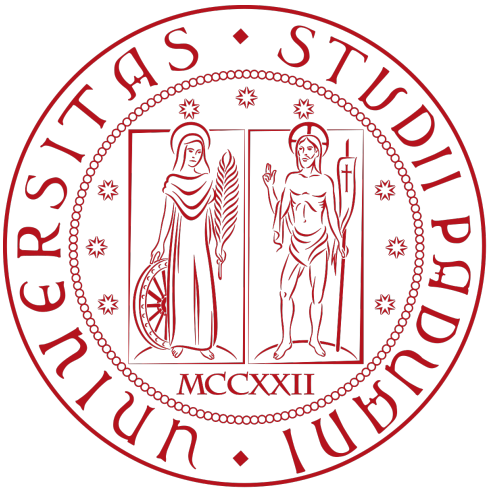

UNIVERSITÀ DEGLI STUDI DI PADOVA

DIPARTIMENTO DI FISICA E ASTRONOMIA

"GALILEO GALILEI"

Corso di Laurea Magistrale in Astronomia

A Photometric and Dynamical Study of the Binary System HW Virginis

Relatore:
Prof. Giampaolo Piotto

Corelatori:
Prof. Valerio Nascimbeni
Dr. Luca Borsato

Laureanda:
Samantha B. Brown Sevilla

Anno accademico 2017/2018

Acknowledgements

I would like to thank all the people that in one way or another inspired me or supported me to pursue becoming an astrophysicist.

A special thanks to my parents, for all of their support and encouragement along this journey, I would not be where I am now without you.

I would also like to thank my supervisor, Valerio Nascimbeni for his guidance, time and patience since the very beginning of this work. I would also like to specially thank Luca Borsato for patiently answering all my questions and being of great help for me to finish this thesis.

I will like to thank as well, all the professors and staff from the AstroMundus programme, taking part of this programme has been one of the best experiences in my life.

Last but not least, I want to thank Pavel Mancera for all his support and words of encouragement whenever I needed them, this would not have been possible without them.

Abstract

The eclipsing binary system HW Virginis is known for its variations of orbital period (ETVs). A planetary system has been proposed as the source of the observed ETVs, but this has not been unambiguously determined, so far. We present a photometric and dynamical study of the system, using new unpublished photometric observations from four different telescopes: the 1.82-m and the Schmidt telescopes from the Asiago observatory; the telescope from "Gruppo Astrofili Salese Galileo Galilei"; and the SuperWASP-South telescope. We found that our eclipse timings are in good agreement within error bars with the timings from the literature, and we increased the existing observations of HW Vir by 10 years. We successfully reproduced the most recent literature model for the binary, nevertheless, we found that this model is unable to fit our new data. Additionally, we tested the stability of the literature model using an N-body integrator and we found the system to be unstable within a few thousand years. As a first attempt to find a model that explains the observations, we used a genetic algorithm to estimate new parameters for the companions of the binary system. We found a set of parameter vectors with a very good fit, able to explain the data, however, these sets of solutions led to masses of the order of brown dwarfs ($\sim 50 M_{Jup}$) and unstable systems. We will explore a different model (one companion plus a quadratic term) to test the feasibility of this solution, as well as alternative or complementary explanations to the ETVs of HW Vir, such as the Applegate effect.

Contents

Acknowledgements iii

Abstract v

Contents vi

1 Introduction 1
- 1.1 Extrasolar planets . . . 1
  - 1.1.1 Techniques to detect extrasolar planets . . . 1
- 1.2 Eclipsing binaries . . . 7
  - 1.2.1 Eclipse timing variations . . . 8
- 1.3 The HW Virginis system . . . 9
  - 1.3.1 Previous studies . . . 9
- 1.4 This thesis . . . 12
  - 1.4.1 Aims and motivation . . . 12
  - 1.4.2 Structure . . . 13

2 Data and Data Reduction 15
- 2.1 Facilities . . . 15
  - 2.1.1 Astrophysical Observatory of Asiago . . . 15
    - 2.1.1.1 The 1.82-m telescope . . . 16
    - 2.1.1.2 The Schmidt telescope . . . 17
  - 2.1.2 The "Gruppo Astrofili Salese Galileo Galilei" telescope . . . 18
  - 2.1.3 SuperWASP . . . 19
- 2.2 Data reduction . . . 20
  - 2.2.1 Preliminary data reduction . . . 20
  - 2.2.2 Final data reduction . . . 20
  - 2.2.3 Time conversion . . . 23

3 Light Curve Fitting 27
- 3.1 JKTEBOP . . . 27
  - 3.1.1 Orbital and physical parameters . . . 28
- 3.2 The *O-C* diagram . . . 29
  - 3.2.1 *O-C* diagram of HW Vir . . . 32

4 Dynamical Modeling **35**
4.1 *LTTE* calculation . . . 35
4.2 Test of the literature model . . . 37
4.3 The search for a new model . . . 39
4.3.1 The `PIKAIA` subroutine . . . 40
4.4 Dynamical stability . . . 49
4.4.1 Dynamical analysis with `Mercury6` . . . 49
4.4.2 `Mercury6` for binaries . . . 50

5 Summary and Conclusions **51**
5.1 Future work . . . 52

List of Figures **52**

List of Tables **55**

Bibliography **57**

Chapter 1

Introduction

1.1 Extrasolar planets

The search for other worlds outside our Solar System has been very fruitful in the past two decades, and, since the discovery of the first exoplanets by Wolszczan and Frail [1992] and Mayor et al. [1995], a wide variety of them has been detected and characterized. Nowadays there are more than 3700 confirmed exoplanets[1], and the number is rapidly rising. From the small rocky ones, to the gas giants of several Jupiter masses (M_J), many have been discovered orbiting Sun-like stars, though, there is an increasing number of exoplanets being discovered orbiting all kinds of stars. One of the most interesting cases is represented by circumbinary planets, which orbit around two stars instead of one. Circumbinary planets can be detected, among other techniques, via the periodic variations in the timing of stellar eclipses in eclipsing binary stars (See Section 1.2.1).

There are several methods to detect exoplanets, both in direct and indirect ways. We will briefly review the most successful ones, giving examples of each one, and emphasizing the method that we used in this thesis in the next Section.

1.1.1 Techniques to detect extrasolar planets

Direct imaging

As it can be inferred from its name, this method consists on actually observing the exoplanets orbiting around a star, by resolving them as light sources. It is currently the only available direct method to detect them. It uses coronagraphy to mask the host star and enhance the contrast between its light and the light reflected or thermally emitted by an orbiting exoplanet, allowing to spatially resolve it (see Fig.1.1). Nowadays adaptive optics also play

[1] http://exoplanetarchive.ipac.caltech.edu/

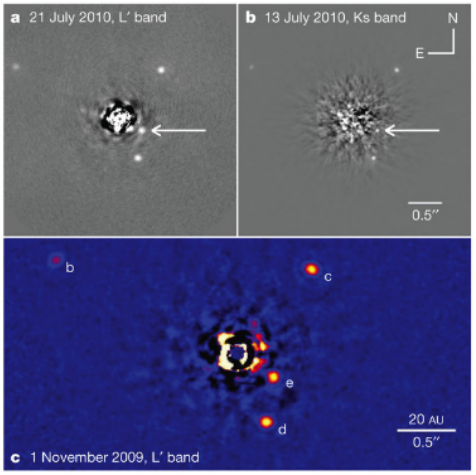

FIGURE 1.1: Near-infrared images of the system HR8799 obtained with the Keck telescope using adaptive optics [Marois et al., 2010]. There are four giant planets, 3 to 7 times M_J.

an important role in this technique, and there have been successful results [Bhattacharya et al., 2018]. Young self-luminous planets orbiting nearby stars are typically the best targets for this method, since they have sufficiently high temperatures (1000-2000 K) and are located in wide orbits ($a > 5$ AU) [Cheetham et al., 2017]. Direct imaging also allows for photometric and spectroscopic studies of the atmospheres of the planets, as we are measuring the photons from the planet itself. It is an excellent complement for other techniques described below, like radial velocity and transits.

Radial velocity

Also known as Doppler spectroscopy, this method measures the reflex radial velocity that an orbiting planet induces on a star, an example of a phase vs radial velocity plot can be seen in Fig.1.2. This technique was one of the first successful methods to detect exoplanets [Mayor et al., 1995]. Radial velocity favors the detection of massive planets, that have a greater gravitational influence on their host stars; as well as the detection of close-in planets, that not only exert a larger gravitational tug, but also have shorter periods, which allows for detections with short-term monitoring. This method allows us to obtain a minimum mass for the planet $M_P \sin i$, provided that the mass of the host star M_* is known, by combining the observed parameters: the velocity semi-amplitude K_*, the period P, the eccentricity e and the argument of the pericenter ω. However, the real mass of the planet depends on the inclination i of the system, which cannot be determined with this method.

Astrometry

This method consists in measuring the position of a star relative to the background sky. In the presence of a planet, the gravitational tug will make the star to move on the sky

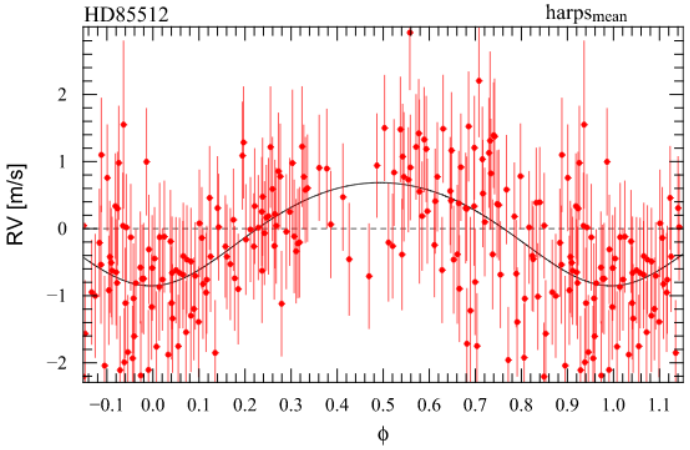

FIGURE 1.2: The phase-folded radial velocity data of HD 85512 and fitted Keplerian solution for the detection of a planet. Figure 13 from Pepe et al. [2011].

over time in a periodic way (see Fig.1.3). Astrometry is more sensitive to planets orbiting nearby stars in wide orbits, as the center of mass displacement amplitude increases with the orbital period. For this reason, astrometry requires measurement stability and precision over a long time base line, which represented a challenge for the available Earth-based instrumentation. However, with the launch of satellites like Gaia [Perryman et al., 2014], the search for planets with this method will become much easier. One of the advantages of this method is that if the stellar mass M_* is known, the planet's mass M_P can be estimated without the need of knowing the inclination i of the system. Therefore, using statistics, this is useful to determine a planet mass function that can contribute to our knowledge of planetary formation. [Maire et al., 2015]

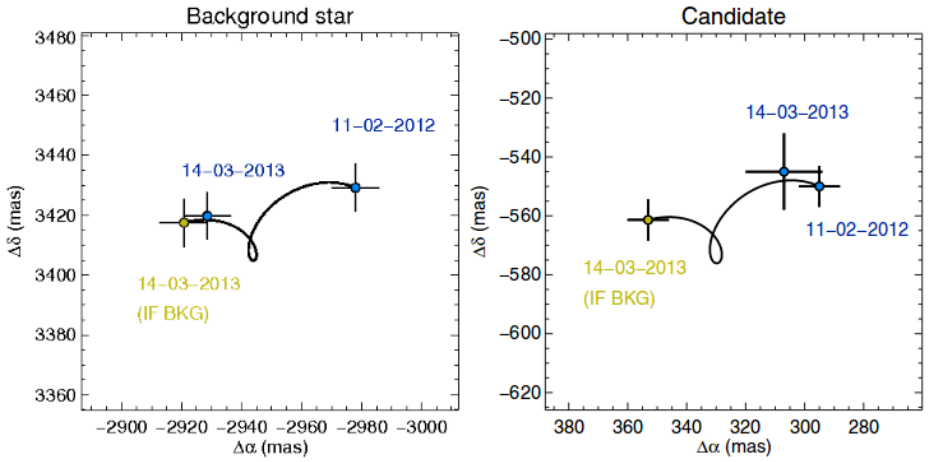

FIGURE 1.3: Top of figure 2 from Rameau et al. [2013]. Right: relative separations between the central star and a candidate companion in right ascension (α) and declination (δ), compared with the position of the companion if it were a background object (in gold). Left: the case of a background star.

Microlensing

For a microlensing event to occur, two stars at different distances should pass within $\sim 1mas$ of each other on the plane of the sky [Gaudi, 2012]. The light from the most distant source star gets bent by the lensing star in between, which in the case of both stars being perfectly aligned along the line of sight, results in the light of the source to be lensed into a ring, thus increasing the apparent brightness of the source star. In the presence of a planet, the planet's own gravity bends the light from the source star and temporarily produces a third image of it. For the observer, this effect appears as two or more peaks (depending on the number of planets that are present) of brightness in the light curve (see Fig.1.4). Among the advantages of microlensing, there is the fact that this is the only method that allows the detection of the furthest and the smallest planets discovered so far; it is most sensitive to planets that orbit in moderate to large distances from their host star, complementing the radial velocity and transit methods. The method allows us to deduce the planet's mass M_P, its orbit, and its period P.

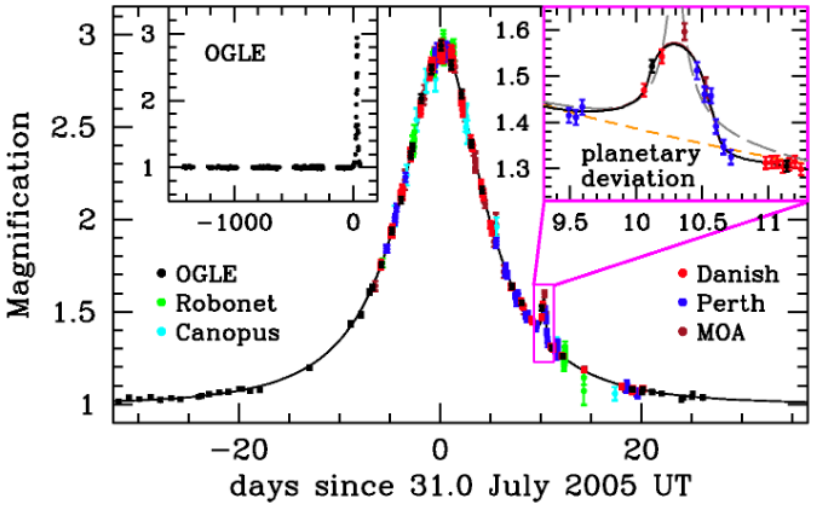

FIGURE 1.4: Light curve of the OGLE-2005-BLG-390 microlensing event along with the best fit model plotted as a function of time. Note the caustic due to the planet in the zoom on the top right. Figure 1 from Beaulieu et al. [2006].

Transits

This method consists in measuring the temporary reduction of the brightness of a star due to a planet passing in front of it, such an event being called a *transit* (see Fig.1.5). Transit light curve analysis allows us to estimate orbital and physical parameters of the system, such as the orbital period P, the limb darkening, and the planet/star radius ratio R_P/R_*, among others. By combining this method with radial velocity, it is also possible to estimate the mass of the planet M_P, and by using spectroscopy, to study the atmosphere's composition of the planet. Transits depend on a lucky geometric configuration. For a planet to transit

its host star, the orbit of the exoplanetary system needs to be nearly "edge-on" from our reference frame. Close-in planets have a higher probability of transiting their host stars, and for this reason, many hot Jupiters have been discovered using this method. Nowadays there are many surveys using this method to detect exoplanets, both ground and space-based (Wheatley et al. [2018], Scandariato et al. [2016]).

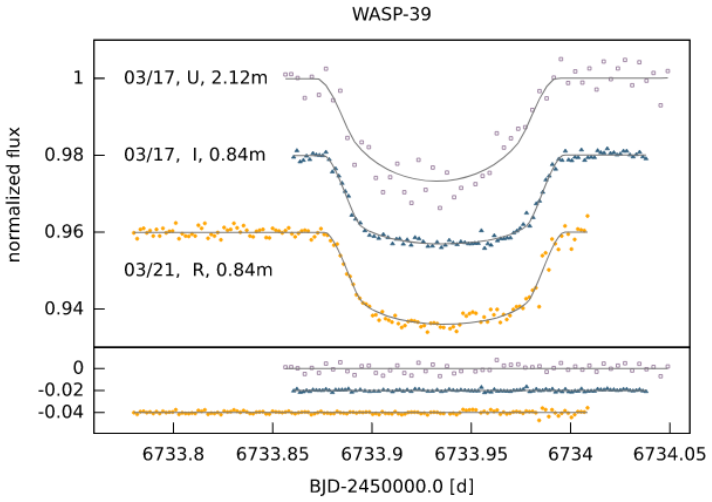

FIGURE 1.5: Light curves of WASP-39b in the U, R and I bands, along with the best fit and corresponding residuals. Figure 3 from Ricci et al. [2015].

Timing

The timing method consists in measuring deviations from a strict periodicity of an otherwise intrinsically regular phenomenon in a star or star remnant. These variations have two main possible sources: the light travel time, and mutual gravitational perturbations. The light travel time effect (LTTE) occurs when the orbit of a star about the center of mass of the star-planet system is sufficiently large that the time light takes to travel through the orbit is detectable as a timing variation. This observed delay is therefore the cumulated effect of a finite signal travel time. When the observable is the orbital period of an eclipsing system, LTTE can arise from the presence of additional bodies, which perturb the orbits of the eclipsing bodies with respect to the barycenter of the system (see Fig.1.6). There are many systems in which timing can be applied to detect exoplanets, such as pulsars, pulsating white dwarfs, pulsating hot subdwarfs, eclipsing binary stars, or even stars with already known transiting planets. In this thesis, we will focus our attention on eclipsing binary stars. The timing method has proved to be successful to detect exoplanets in all the above mentioned systems, and it was also the method utilized to detect the first exoplanets [Wolszczan and Frail, 1992].

The fundamental tool for timing analysis is the so called *Observed minus Calculated* or *O-C* diagram, which we describe in detail in Section 3.2. In Fig. 1.6 we see an example of these kind of diagrams, showing the observed minus calculated eclipse timings as a function of

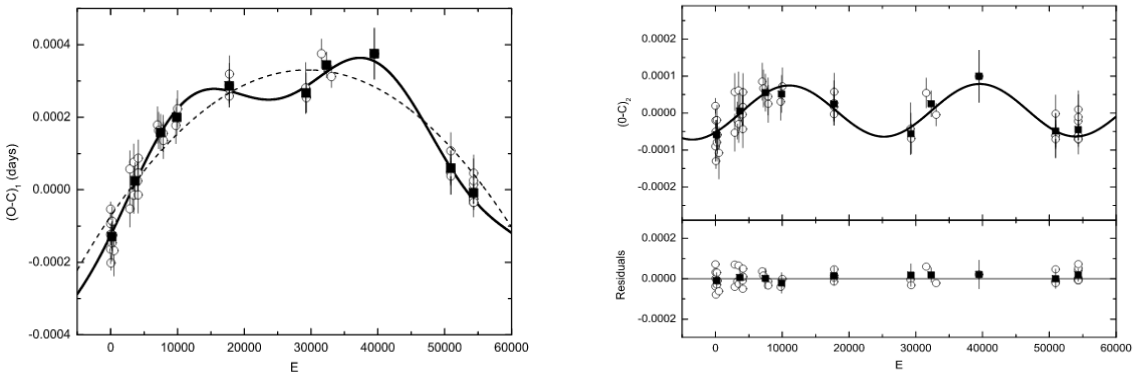

FIGURE 1.6: Left: Observed-calculated (*O-C*) diagram (see text and Section 3.2) of the eclipsing binary NY Vir. Right: light-travel-time effect due to the supposed presence of a giant circumbinary planet in NY Vir, after subtraction of the downward parabolic change from the O-C diagram on the left. Figures 2 and 3 from Qian et al. [2012].

the *epoch* (see Section 3.2). It is with these diagrams that we are able to tell whether there are changes in the period of an object or system, or not. To construct an *O-C* diagram it is necessary to use a stable an accurate astrophysical "clock", which will depend on the system we are studying.

There are two classes of techniques based on timings:

Kinematical: where the changes of position of an astrophysical "clock" with respect to the barycenter of the system are measured through the LTTE (which translates difference of positions into time delays). This technique works even when the planets are not significantly interacting with each other, as well as with only just one planet because, in general, the "clock" does not coincide with the barycenter. This is described by Equation 4.3 [Irwin, 1952].

Dynamical: where the mutual gravitational perturbation of three or more bodies result in deviation from an ideal Keplerian motion with constant orbital elements. Transit timing variations or TTVs fall within this classification. This technique requires two or more transiting and mutually interacting planets, and unless in very particular orbital configurations, the problem requires extremely intensive N-body numerical integration to be solved.

The only common aspect between the two techniques is that they are based on the measurement of a periodic phenomenon, since they widely differ in terms of sensitivity, biases, applicability, etc.

1.2 Eclipsing binaries

A binary system is composed by two stars that orbit their common center of mass. It is usual to refer to the brighter star as the *primary* star, and to the dimmer of the two as the *secondary* star. Binary stars can be classified according to the way we observe them, as *visual*, *spectroscopic*, *astrometric* or *eclipsing* binaries; or by the size of their orbits, as *wide orbit* or *close orbit* binaries. In this thesis we will focus our attention on the eclipsing binaries. A further classification, according to whether or not the stars fill their own Roche lobes[2] and whether or not they are in contact with each others lobes, groups them into *detached*, if each star is within its own Roche lobe; *semi-detached*, if one of the stars completely fills its own Roche lobe; and *contact*, if both stars exactly fill their own Roche lobes.

Eclipsing binaries are a special case in which the orbital plane of the binary system lies approximately edge-on to the line of sight so that each star will be seen to eclipse each other every orbital period. These type of binaries are detected via photometric measurements, by looking for a periodic change in the light curve of the system. The light curve of an eclipsing binary has two minima, a deep minimum when the brighter star is eclipsed, and a shallower minimum when the fainter star is eclipsed, called the primary and secondary eclipses, respectively. Many important physical and orbital parameters can be estimated from analyzing the light curves of eclipsing binary stars, specially when combined with radial velocity measurements, such as the stellar masses and radii, as well as the period, the eccentricity, the orbital inclination, and even the temperature of the stars. Another purpose that eclipsing binaries have been used for is to make distance estimates [Pietrzyński et al., 2013].

By studying these systems, some interesting unexpected structural details and time-related changes in the component stars have been discovered. Examples of them include: dark or bright spots on the surface of the stars, similar to but much larger than the ones found on the Sun; stars shaped as ellipsoids due to their rapid rotation; stars that appear brighter as mass is exchanged from one companion to another, etc. All of the above has helped to compute stellar parameters and test stellar evolution models [Southworth, 2012b].

Binary systems can be composed by a variety of stellar types, however, in this work, we will focus our attention on a particular kind of eclipsing binaries, the subdwarf B/O and main-sequence M star (sdB/O + dM) binaries or, HW Virginis binaries, and more specifically in the first system of this kind ever discovered, i.e. HW Virginis itself (Section 1.3). These systems are pre-cataclysmic, and will therefore undergo mass transfer in a few thousand million years [Wood et al., 1993].

A subdwarf star belongs to the luminosity class VI, with a luminosity that is 1.5 to 2 magnitudes below the luminosity of a main-sequence star of the same spectral type. Hot subdwarfs, of spectral types O and B, are core helium-burning stars at the blue end of the horizontal

[2]The Roche lobe of a star in a binary system is the area in which the gravitational pull of the star is greater than the gravitational pull of its companion.

branch (also called "extreme horizontal branch stars"). Many of this stars have been discovered to belong to binary systems, usually with white dwarfs or low-mass main-sequence stars as companions [Han et al., 2002].

1.2.1 Eclipse timing variations

If we neglect non-gravitational forces (such as tides) the orbit of an isolated, unperturbed binary star system is purely Keplerian, i.e. with constant orbital elements. In such systems, the orbital evolution can be analytically predicted. For an eclipsing binary system this means that its eclipses will happen at strictly regular intervals and will have the same duration every time. However, if the system is perturbed in any way, it will show changes in the period of the eclipses, known as Eclipse Timing Variations (ETVs).

There are a number of processes that can be responsible for these variations, for example, the presence of additional bodies, like exoplanets or (sub)stellar companions, can cause eclipses to appear earlier or later than expected (see LTTE in *Timing*), and change the period of the binary over time. These planets may have formed together with the binary system, in which case they are called *first-generation* planets; or, they may have formed after the system evolved and underwent a common envelope phase, in this case they are called *second-generation* planets or *post-common-envelope* (PCE) planets; there also exists the possibility of a hybrid scenario in which the already existing planets may have accreted the expelled gas from the stars [Heber, 2016]. As we briefly mentioned in Section 1.1, exoplanets discovered to orbit this kind of systems are of particular interest, since they provide insight not only into the binary star, but also regarding the planet formation theories [Smullen et al., 2016].

There are also other processes to explain ETVs that do not invoke the presence of additional bodies, in the following section we describe the most relevant one for the elaboration of this work.

The Applegate effect

This effect, proposed by Applegate [1992], describes the ETVs as a result of the magnetic activity in one of the members of the binary system. According to Applegate, the distribution of the angular momentum in the active star changes as the star goes through its activity cycle, these variations on the angular momentum distribution produce variations in the gravitational quadrupole moment of the star, i.e. in the shape of the star, making it more or less oblate, which traduces in changes in the orbit of the system and thus, in the orbital period.

There have been a number of studies regarding this effect in the recent years (Völschow et al. [2016], Schleicher and Mennickent [2017], Navarrete et al. [2018], among others), where the feasibility of it being the cause behind the ETVs strongly depends on the energy

budget of the magnetic star of the system, and therefore, for some systems, this effect might not be the only cause behind the ETVs. More recently, Völschow et al. [2018] presented a more detailed approach to study the kinetic and magnetic fluctuations that give raise to the modulation period, and their findings support the previous reported conclusion of the Applegate effect not being sufficient to produce alone the observed variations in systems with TTVs. This leads us to the conclusion that both kinds of processes, i.e. involving additional bodies or not, are not mutually exclusive, and they can both contribute to different levels to explain the ETVs.

1.3 The HW Virginis system

HW Virginis (hereafter HW Vir) is a detached, pre-cataclysmic, eclipsing binary system, first identified as a UV-bright object by Carnochan and Wilson [1983] and later, claimed as a binary by Menzies and Marang [1986]. Its equatorial coordinates ($J2000$) are α : 12h 44 min 20.24s and δ : $-8°40'16.84''$, the system has a very short period of only 2.8 h, and it is composed by a subdwarf B (sdB) and a main sequence M star (dM), with masses 0.485 $M_\odot$ and 0.142 $M_\odot$, and radii 0.183 $R_\odot$ and 0.175 $R_\odot$, respectively (see Table1.1 for the most recent parameters). It was the first ever discovered sdB+dM binary, which made it the prototype for all the later discovered binaries of this kind (i.e. sdB+dM binaries with short periods ∼0.1 day). A simulated image of the binary system can be seen in Fig. 1.7.

1.3.1 Previous studies

A decrease in the orbital period of the system was first studied by Kilkenny et al. [1994], by analyzing eclipse timings over a 9 yr baseline. They concluded that the best mechanism to explain this effect was the nowadays called Applegate effect (see Section 1.2.1), however, they did not rule out the possibility of a third body in the system to be the underlying cause for the period variations, but left this hypothesis to be tested via future observations. Çakirli and Devlen [1999] re-analyzed the eclipse timings between 1984-1999 and concluded that the mechanism behind the period variations was the LTTE, and proposed that HW Vir was revolving about a third body with a period of 19 yr. Later on, other authors (Wood and Saffer [1999], Kilkenny et al. [2000], Kiss et al. [2000]) analyzed the period variations with different techniques, but did not arrived to a conclusive explanation for the ETVs.

A few years later, Kilkenny et al. [2003] presented new eclipse timings for HW Vir and confirmed the presence of a periodic term, supporting their idea of a third body in the system, revolving around the common center of mass between it and the binary. They proposed this body to be in the *brown dwarf* mass range (0.028 $M_\odot$) and the period of the orbit to be 20.7 yr. İbanoğlu et al. [2004] continued to study HW Vir with photometric

Parameter	Primary		Secondary	Reference
Orbital period P (days)		$0.11671967 \pm 1.15 \times 10^{-7}$		Beuermann et al. [2012]
Separation a ($R_\odot$)		0.860 ± 0.010		Lee et al. [2009]
Inclination i (°)		80.98 ± 0.10		Lee et al. [2009]
Eccentricity e		<0.0003		Beuermann et al. [2012]
Distance d (pc)		181 ± 20		Lee et al. [2009]
Mass ($M_\odot$)	0.485 ± 0.013		0.142 ± 0.004	Lee et al. [2009]
Radius ($R_\odot$)	0.183 ± 0.026		0.175 ± 0.026	Lee et al. [2009]
Temperature (K)	28488 ± 208		3084 ± 889	Wood and Saffer [1999] and Lee et al. [2009]
Bolometric magnitude M_{bol} (mag)	1.46 ± 0.24		11.20 ± 0.46	Lee et al. [2009]
Visual magnitude M_V (mag)	4.22 ± 0.24		15.59 ± 0.46	Lee et al. [2009]
Bolometric luminosity L_{bol} ($L_\odot$)	19.7 ± 5.6		0.003 ± 0.001	Lee et al. [2009]

TABLE 1.1: HW Virginis orbital and physical parameters from the literature.

observations and arrived to the same conclusion, the third body being a brown dwarf.

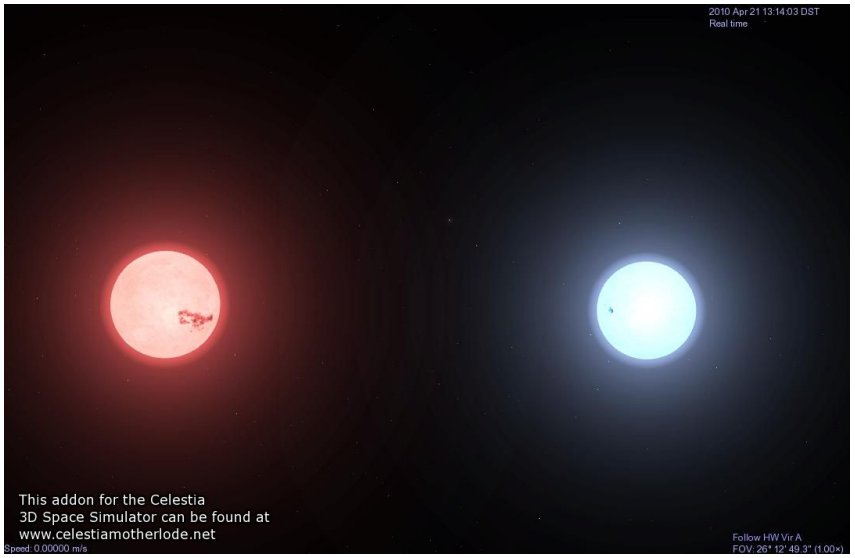

FIGURE 1.7: HW Vir simulated with the Celestia 3D Space Simulator http://celestiamotherlode.net/

Lee et al. [2009] reported new CCD photometry for a timebase of 8 yr and proposed that the continuous period decrease may be caused by angular momentum loss due to magnetic stellar wind braking[3] and that the cyclic period variations may be explained by the presence of two additional bodies in the system, of masses $M_3 \sin i_3 = 19.2 M_J$ and $M_4 \sin i_4 = 8.5 M_J$, respectively. This model was tested by Beuermann et al. [2012], who found that it did not fit their new eclipse timings (as seen in Fig. 1.8). They also tested the stability of Lee et al.'s model and found it unstable within a few thousand years. Beuermann et al. proposed a new model with two companions of masses $M_3 \sin i_3 \simeq 14 M_J$ and $M_4 \sin i_4 = 30 - 120 M_J$, and periods of 12.7 yr and 55 ±15 yr, respectively. Horner et al. [2012] on their own, analyzed Lee et al.'s model and arrived to the same conclusion of it not being stable on very small timescales, notwithstanding, they concluded that the ETVs are not only driven by gravitational influence of perturbing planets, and that there must be another mechanism taking place in order to explain them.

A recent paper [Navarrete et al., 2018], discarded the possibility of the Applegate effect as the underlying cause for the eclipsing time variations of HW Vir, by calculating the required energy to produce the observed ETVs via magnetic activity and finding that the magnetically active star (the dM star) is not energetic enough to produce these variations.

So far, a conclusive explanation for the observed timing variations of HW Vir is still missing.

[3] Angular momentum loss by magnetic braking occurs when ionized material from the star gets captured by the magnetic field lines and eventually carried away from the star through the stellar wind, causing the star to slow down its spin.

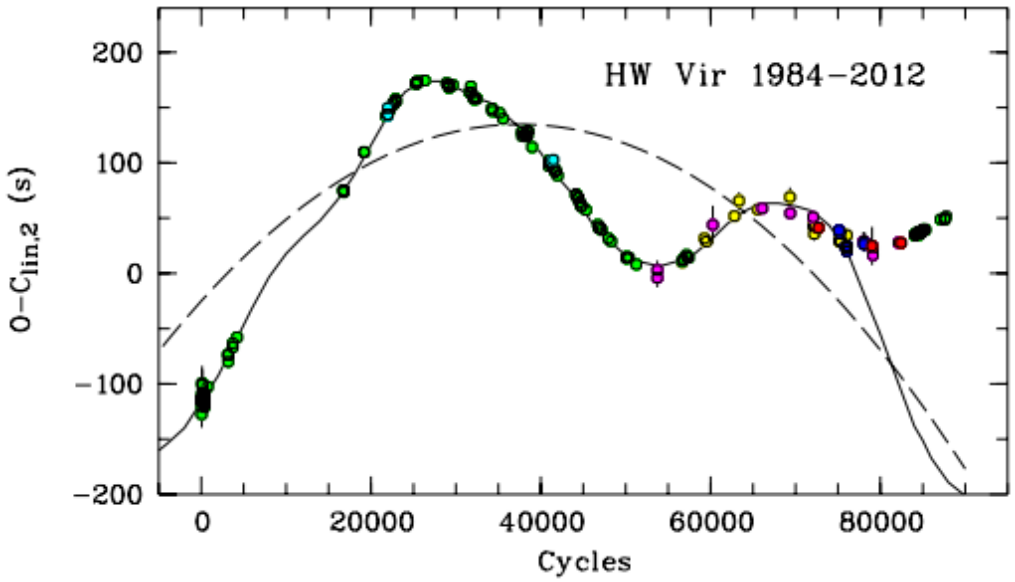

FIGURE 1.8: Figure 1 from Beuermann et al. [2012]. Observed minus calculated (*O-C*) diagram of HW Vir after subtracting the eclipse times from the linear ephemeris used by Lee et al. [2009], along with their two-companion model (solid curve) and the underlying quadratic ephemeris (dashed parabola). The diagram was built using data from SAAO (green), Wood et al. (cyan), Lee et al. (yellow), BAV and VSNET (magenta), AAVSO (blue), BRNO (red), and MONET/North (dark green).

1.4 This thesis

1.4.1 Aims and motivation

As we discover more and more exoplanets around different kinds of stars, the number of unknowns also rises, since there is still a lot to clarify and add to the theory of formation and evolution of planets. On the other hand, systems like HW Vir represent a group of candidates to planetary systems with growing evidence, and uncovering the underlying causes of its period variations in an unambiguous way may also set a benchmark for all the other members of this class and give us some insight in the fate of planets around evolved binary systems.

So far, the presence of additional bodies to the HW Vir system has proven to be the most plausible explanation for its ETVs. Therefore, the aim of this work is to derive new eclipse timings from our photometric data, and use them along with the literature timings to provide a better estimation of the parameters of the companions of HW Vir, as well as to test these new parameters for stability on a large timescale.

1.4.2 Structure

In Chapter 2 we describe the facilities that were used to obtain our photometric data, as well as the data reduction process we followed for each dataset and the time conversions that were needed for the purposes of this work. In Chapter 3 we give details about the software we used to fit the light curves, we define the orbital and physical parameters of binary systems, and we present new eclipse timings obtained from our data, as well as our results for the *O-C* diagram and its implications. In Chapter 4 we give details about the software we used to test the literature model for the LTTVs of HW Vir, as well as the code used for the dynamical analysis of the binary and its companions, and we present the results from our new analysis. Finally, in Chapter 5 we summarize our conclusions and describe the future work.

Chapter 2

Data and Data Reduction

In this Chapter we describe our data and the process we followed to reduce each of the datasets. In Section 2.1, we present the instrumentation used to obtain the unpublished photometric observations of HW Vir presented on this thesis. Then in Section 2.2, we describe our data as well as the process we followed to reduce it according to its source.

Our data consists of photometric observations of HW Vir covering a timespan of ∼10 years, from 2008 to 2018, and it was obtained using the different facilities described below.

2.1 Facilities

2.1.1 Astrophysical Observatory of Asiago

The Astrophysical Observatory of Asiago is located in the northern part of Italy. It hosts three optical telescopes: a 1.22-m telescope, at a latitude of 45°51′59″N, a longitude of 11°31′35″E, and an elevation of 1044.2 m, dedicated to Galileo Galilei and operated by the University of Padova since 1942; and two other telescopes located a few kilometers away at the observing station of Mount Ekar (45°50′40″N of latitude, 11°34′22″E of longitude and an elevation of 1370 m), the 1.82-m telescope[1], dedicated to Nicolas Copernicus; and the Schmidt telescope[2]. These last two telescopes are operated by INAF (Istituto Nazionale di Astrofisica) and were used to obtain part of our data. Below we give a more detailed description of them.

[1] http://www.oapd.inaf.it/index.php/en/telescopes-and-instrumentations/copernico-telescope-1-82.html

[2] http://www.oapd.inaf.it/index.php/en/telescopes-and-instrumentations/schimidt-telescope-67-92.html

2.1.1.1 The 1.82-m telescope

This telescope (shown in Fig. 2.1) has been in operation since 1973, it is a Cassegrain reflector with a primary mirror of 1.82-m, making it the largest optical telescope within Italian territory. It has an *equivalent focal length* of $f/9$, which corresponds to an image scale of 12.6 $''$/mm. There are two instruments available at this telescope: a high resolution Echelle spectrograph, and the low resolution Asiago Faint Object Spectrograph and Camera (AFOSC[3]), which was used to obtain our data. The current CCD of AFOSC has a *field of view (FoV)* of $9'$ x $9'$, a *read-out noise (RON)* of $\sim$7.6 e^- and a *gain* of 2.7 e^-/ADU. The CCD is a $2k$ x $2k$ (2048 x 2048) detector with a scale of $0.26''$/pixel and a wavelength coverage range of 330-1100 nm. It is equipped with a set of Bessel *UBVR* filters and a set of Gunn *ugriz* filters, from which the *V*, *R* and *r* were used to obtain our data. We have a total of twelve light curves of HW Vir obtained with this telescope within the TASTE observing campaign (PI: Nascimbeni et al. [2011]). The defocusing technique was used to obtain our data. This manner of performing photometry has the advantage of allowing long exposures on bright stars, which reduces the scintillation noise and results in a lower Poisson noise due to the large number of photons collected.

FIGURE 2.1: The 1.82-m telescope at Mount Ekar. Picture taken from http://www.oapd.inaf.it/index.php/en/telescopes-and-instrumentations/copernico-telescope-1-82.html).

[3] http://www.oapd.inaf.it/index.php/en/telescopes-and-instrumentations/copernico-telescope-1-82/136-asiago-eng/250-afosc.html

2.1.1.2 The Schmidt telescope

The Schmidt telescope was built in 1966 and it was moved from its original position at the Astrophysical Observatory of Asiago in 1991, in order to seize the higher altitude and lower light pollution of Mount Ekar (see Fig. 2.2). This telescope has a 67 cm diameter correcting plate in UBK7 Schott glass, a 91 cm diameter spherical mirror in Duran-50 Schott glass, and it has a focal length of 215 cm, which gives an *equivalent focal length* of f /3.2, corresponding to an image scale of 95.9 $''$/mm. The CCD in current use has a scale of 0.87 $''$/pixel (unbinned), a pixel size of 9 µm, and a *FoV* of 59$'$ x 59$'$, the full-frame read out time is of 22 s, the *RON* of 10 e^- and the *gain* of 1.6 e^-/ADU. A filter wheel is available with *B* and *V* Johnson-Bessel, and *ugri* Sloan filters. Our data was taken using the *R* and *r* filters within the TASTE observing program (PI: Nascimbeni). We have three light curves of HW Vir from this telescope, one of them obtained in April 2018, being the most recent one of the whole dataset.

FIGURE 2.2: The Schmidt 67/92 telescope dome at Mount Ekar. Picture taken from http://www.oapd.inaf.it/images/immagini_asiago/schimdt60_90_not.jpg).

Night date	Frames	Filter	Eclipse	Origin
2011/02/05	330	R-Bessel	Partial primary	Copernico
2012/01/26	1520	V-Bessel	Both eclipses	Copernico
2013/02/04	448	V-Bessel	Primary	Copernico
2013/02/07	930	V-Bessel	Both eclipses	Copernico
2014/03/06	1357	V-Bessel	Primary	Copernico
2014/04/01	1088	V-Bessel	Primary	Copernico
2015/03/13	324	r-Sloan	Partial primary	Copernico
2016/02/05	621	V-Bessel	Primary	Copernico
2016/02/08	1292	V-Bessel	Both eclipses	Copernico
2017/01/21	1977	r-Sloan	Primary	Copernico
2017/02/25	1682	r-Sloan	Both eclipses	Copernico
2017/03/02	984	r-Sloan	Primary	Copernico
2012/03/11	321	R-Bessel	Both eclipses	Schmidt
2012/03/12	339	R-Bessel	Both eclipses	Schmidt
2018/04/20	558	r-Bessel	Primary	Schmidt
2014/03/12	282	V-Bessel	Both eclipses	GAS
2014/03/28	728	V-Bessel	Both eclipses twice	GAS
2014/03/29	660	V-Bessel	Both eclipses twice	GAS
2014/03/30	304	V-Bessel	Both eclipses	GAS
2014/03/31	700	V-Bessel	Both eclipses twice	GAS
2014/05/24	325	V-Bessel	Both eclipses	GAS

TABLE 2.1: HW Virginis observations indicating the dates, number of science frames, filter used, number of eclipses in the light curve and source of the data.

2.1.2 The "Gruppo Astrofili Salese Galileo Galilei" telescope

This telescope is located at the town of Santa Maria di Sala, in northern Italy (45°30′8″N latitude and 12°1′29″E longitude) and it is operated by a local group of amateur astronomers[4]. It is a Newtonian telescope with a primary mirror of 410mm of diameter, and a focal length of 1710mm. The CCD is equipped with a Kodak KAF1600 ME sensor and it can be cooled down to nearly −60°C. The pixel size is of 9 x 9 μm and the scale of 1.09″/pixel. The imager includes a filter wheel with Bessel *BVRI* filters. With the help of the "Gruppo Astrofili Salese Galileo Galilei" (GAS) and in particular of Francesco Scaggiante, we obtained six light curves of HW Virginis in the *V* filter.

We resume the information of the unpublished observations in Table 2.1, where we include the date of the observing night, the number of science frames taken, the filter in which the observations were made, which and how many eclipses are seen in the light curve, and the source of the data.

[4] http://www.grag.org/

2.1.3 SuperWASP

The SuperWASP (*Wide Angle Search for Planets*) survey is an automatized search for exoplanets using the transit method [Pollacco et al., 2006]. The detection program is coordinated by the Isaac Newton Group (ING), the Instituto de Astrofísica de Canarias (IAC), and six universities from the United Kingdom. It consists of two robotic observatories that operate continuously throughout the year, one in the northern hemisphere and one in the southern hemisphere, which allows a coverage of all the sky. The first observatory, SuperWASP-North, is located on the island of La Palma, Canary Islands, and it is part of the ING facilities. The second observatory, SuperWASP-South, is located at the site of the South African Astronomical Observatory (SAAO), outside Sutherland, South Africa. Each observatory consist of eight Canon 200mm f1.8 lenses, backed by wide-angle CCD cameras of 2000 x 2000 pixels of resolution (see Fig.2.3), that simultaneously monitor the sky for planetary transit events.

Our largest dataset of HW Vir comes from SuperWASP-South: 4 years of observations of HW Vir from 2008 to 2012, which gives a total of 353 light curves. This particular dataset has not yet been included in the public SuperWASP data release, and has been kindly provided to us by the WASP team.

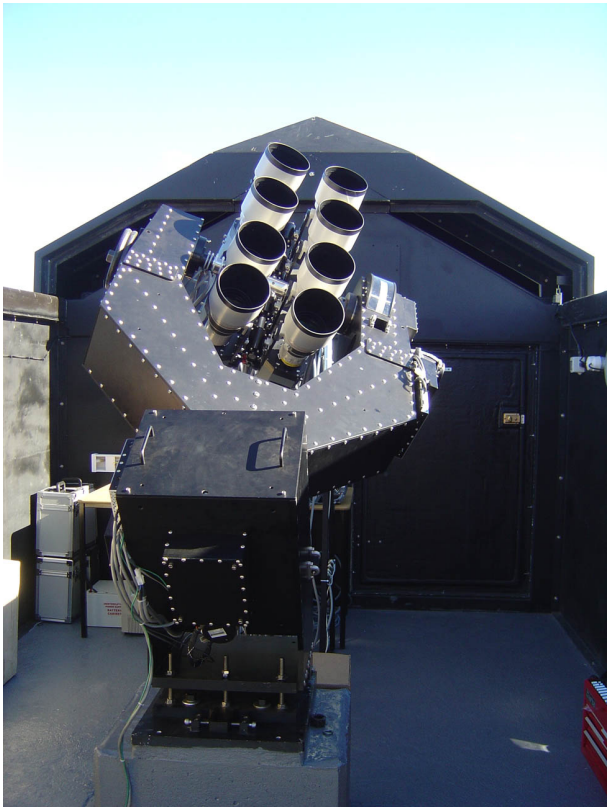

FIGURE 2.3: The SuperWASP-South cameras. Picture taken from https://wasp.cerit-sc.cz/form).

2.2 Data reduction

2.2.1 Preliminary data reduction

For all our data, except for the SuperWASP nights, we performed the data reduction starting from the raw CCD images in the usual way, by performing standard pre-reduction procedures. In order to do so, two kinds of images are taken along with the observations, *bias* and *flat-field* images. The first ones measure the charges left on the CCD even with the shutter closed and 0 s of exposure time. The presence of these charges is related to the fact that a finite direct current is needed to move the charges from the pixels to the output register, and this introduces a bias in the science frames. The second ones measure the response of each pixel in the CCD to a homogeneous, *flat* illumination. These images correct for the variations in illumination in the field that may be introduced by dust in the mirrors or filters, CCD inhomogeneities, optical vignetting, or other effects. We used the `STARSKY` code to perform the data reduction. `STARSKY` is a pipeline written in *Fortan 77/90* by Nascimbeni et al. [2011], [2013], and was specially developed for The Asiago Search for Transit timing variations of Exoplanets (TASTE). `STARSKY` features different subroutines for each step of the data reduction; to generate both the *master bias* and *master flat-field* frames corresponding to each night and perform the image correction, we used the `HUGGY` subroutine.

Once the images were corrected, we used the `SENTINEL` subroutine to perform a photometric extraction at a glance and to get a preliminary light curve for each night. These preliminary light curves are shown in Fig.2.4, Fig.2.2, and Fig.2.6, for the Copernico, Schmidt, and GAS datasets, respectively.

2.2.2 Final data reduction

For the data reduction we used the differential aperture photometry technique, due to the conditions under which most of our data were acquired, i.e. defocussing the images, with the seeing of the sites causing a highly variable PSF[5], and the lack of stellar crowding in the field of HW Vir (see Fig.2.7a). Compared to "absolute" photometry, differential photometry is more accurate since it minimizes the error introduced by variations in the atmosphere (i.e. atmospheric extinction). By obtaining measurements of the target star along with one or more reference stars, magnitude (or flux) differences (ratios) of the target relative to the reference stars can be determined and the changes in the luminosity are revealed. In more detail, this technique consists in selecting a circular aperture around the target star as well as an inner and outer ring that encircle the background sky close to the star (see Fig. 2.7b), and then summing up the pixel counts within the aperture, and subtracting the average count value of the pixels within the ring (the average sky value), divided by the

[5]Point Spread Function.

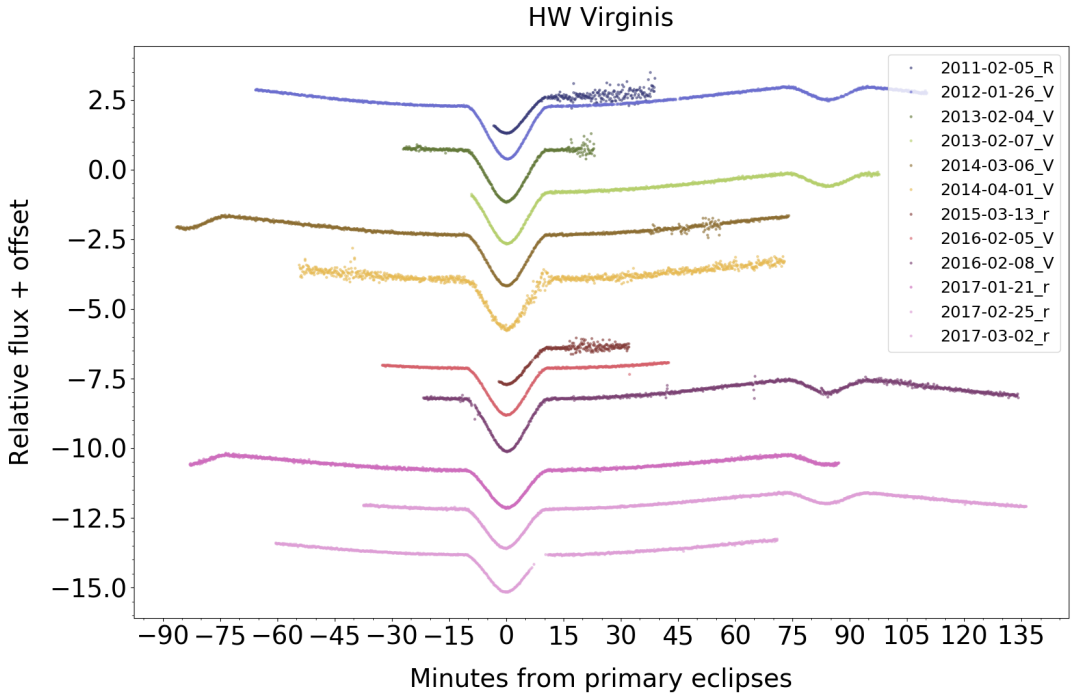

FIGURE 2.4: Light curves obtained from the photometric observations of the Copernico (1.82-m) telescope in three different filters, R, V and r. The depth of the eclipses varies according to the filter. The light curves are shifted in flux for visualization purposes.

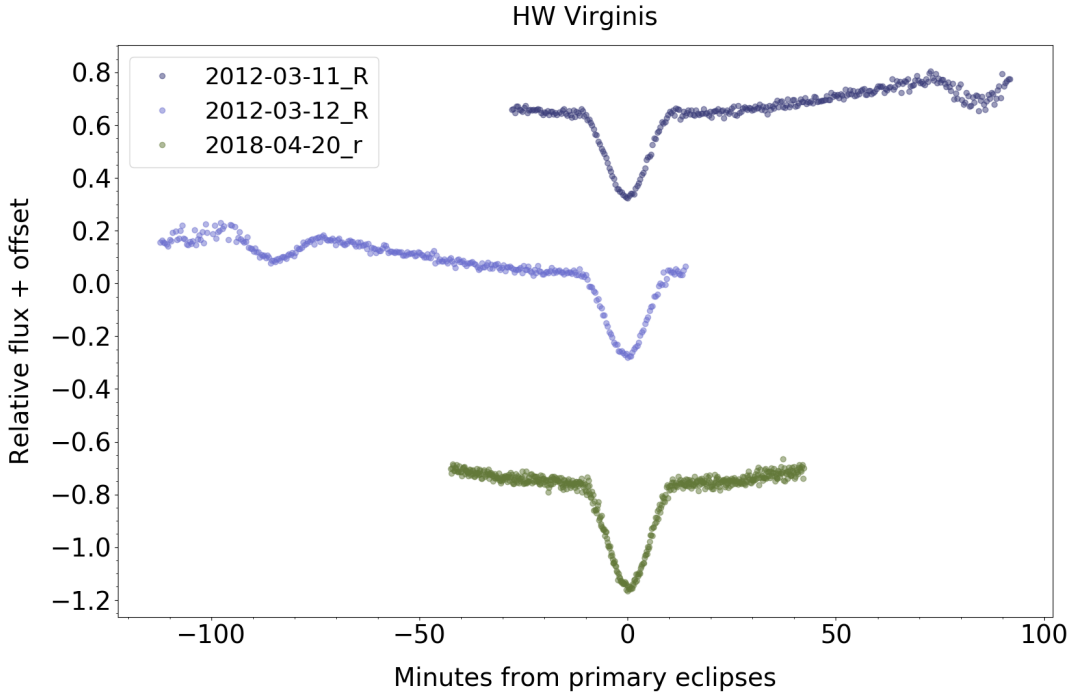

FIGURE 2.5: Light curves obtained from the photometric observations of the Schmidt telescope in the R and r filters. Shifted in flux for visualization purposes.

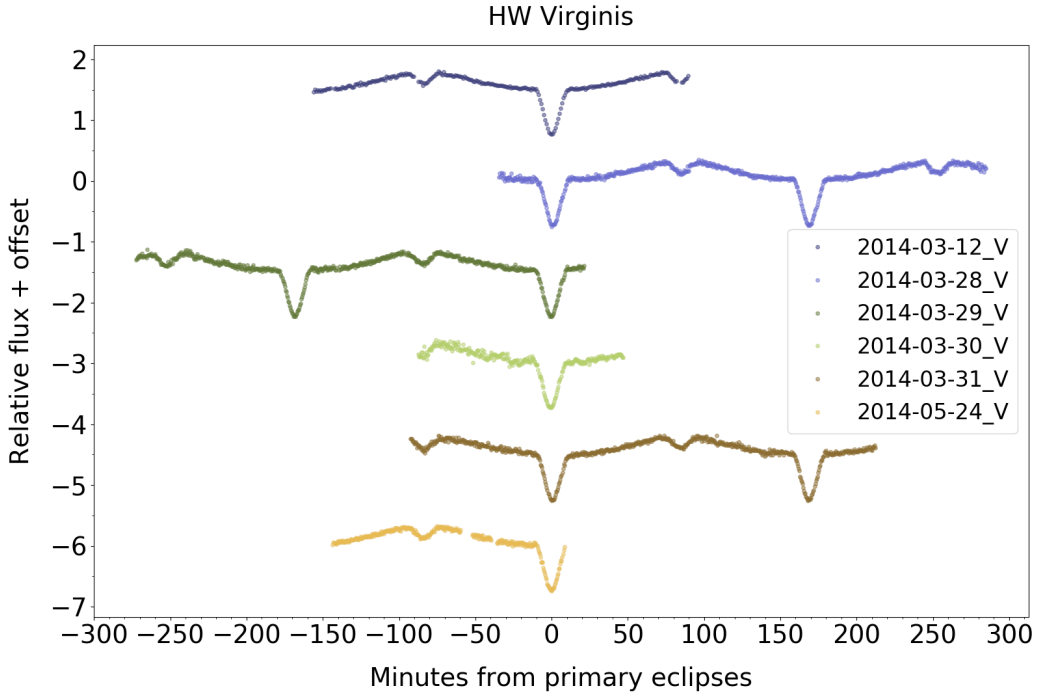

FIGURE 2.6: Light curves obtained from the photometric observations of the GAS telescope in the V filter. Shifted in flux for visualization purposes.

number of pixels within the aperture, to get the raw flux value of the star. This process is repeated for the reference stars in the field, and the resulting raw fluxes are divided by each other to obtain the final differential flux (all of the above is performed in an automatic way within the software). In our case we used different reference stars according to the field covered by each telescope. An example of the field of the Schmidt telescope showing HW Vir along with the used reference stars can be seen in Fig.2.7.

The STARSKY software allows us to perform differential photometry as well, and as an output it provides five different light curves derived from five different aperture choices, indicating the one with the smallest empirical RMS[6], therefore minimizing any systematic errors.

In the particular case of SuperWASP, the data was already reduced, therefore none of the above steps were necessary to obtain the light curves. However, to make it easier to work with, we divided the large dataset (2008-2012) into four parts ("seasons") corresponding to each year of observations. In Fig.2.8 we present the co-added, folded light curves from these four seasons.

[6]Root Mean Square.

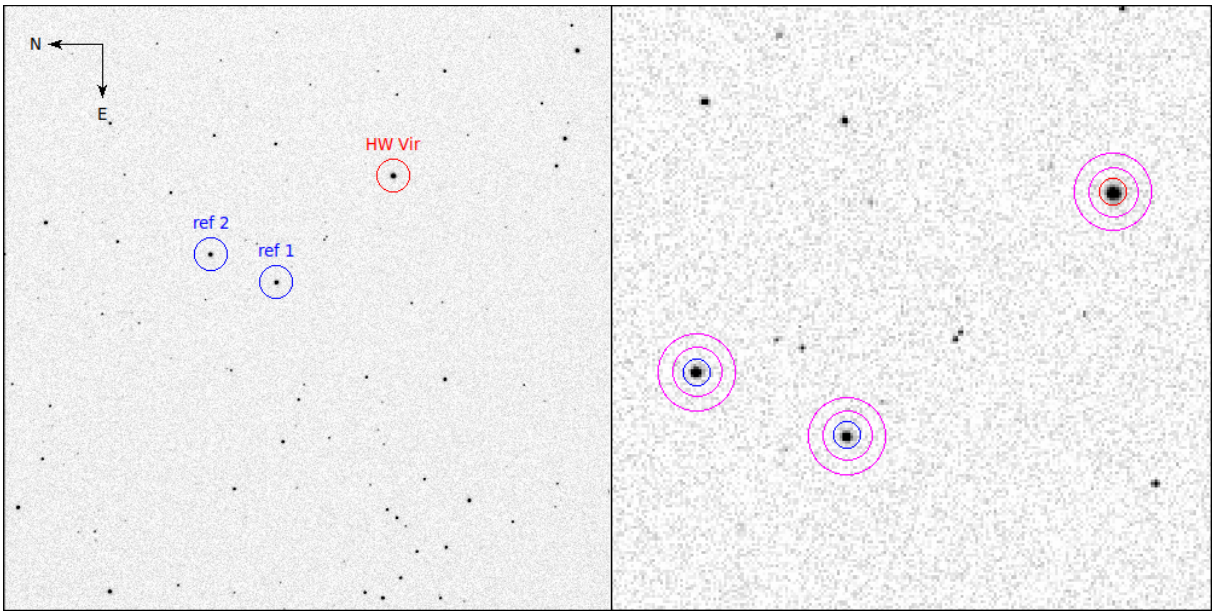

(A) (B)

FIGURE 2.7: HW Vir field. (A): Example of a typical frame obtained with the Schmidt telescope, size 15′ x 15′. The target and the reference stars are indicated in red and blue, respectively. (B): Zoom of the left image, the magenta circles indicate the inner and outer rings used to estimate the background level.

2.2.3 Time conversion

An important aspect in the measurements of any astronomical event, is an accurate measurement of the time. This aspect becomes crucial when trying to measure variations with an absolute accuracy better than 1 minute, as in the case of ETVs. For this reason, it is advised to convert to the most stable time stamp system[7] available, i.e. the *Barycentric Julian Date* as a reference frame, in the *Barycentric Dynamical Time* standard, or BJD_{TDB} [Eastman et al., 2010]. The BJD refers to the Julian Date[8] corrected for differences in the Earth's position with respect to the barycenter of the Solar System. And the TDB is the Terrestrial Time[9] (TT) corrected for general relativity effects.

This aspect was fundamental for us given the large time baseline of our data, since any error in the time stamp of the observations could accumulate over the years giving spurious results for the eclipse timings. Among the data we analyzed, there are time stamps reported in both BJD in *Coordinated Universal Time* or BJD_{UTC}, and in *Heliocentric Julian Date* in UTC or HJD_{UTC}. To convert them to BJD_{TDB} we used the program `VARTOOLS`[10], which is a command line resource that, among other implementations, includes an option to convert between time stamps.

[7] The time stamp is the combination of a reference frame and a time standard.

[8] The Julian date is the number of elapsed days since the beginning of a cycle of 7,980 years starting on January 1, 4713 B.C.. It was invented by Joseph Scaliger in 1583.

[9] See Eastman et al. [2010] for further information on time standards.

[10] `https://www.astro.princeton.edu/~jhartman/vartools.html`

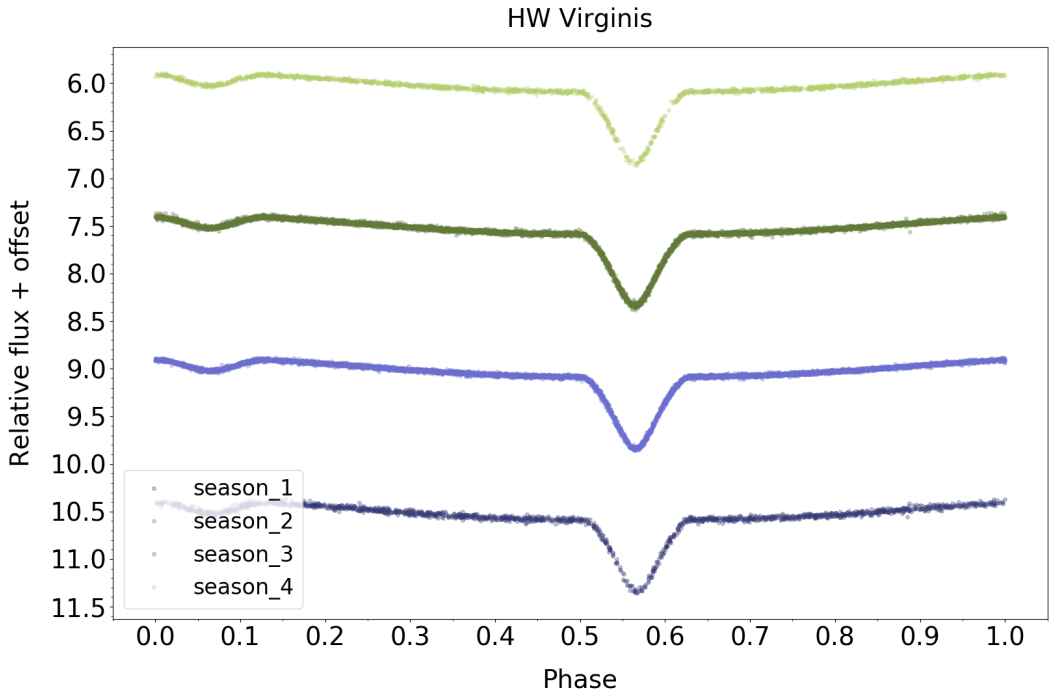

FIGURE 2.8: Light curves obtained from the photometric data of the SuperWASP consortium. Here the data was split in four "seasons" corresponding to each year of observations. The light curves are shifted in flux for visualization purposes.

Due to the critical importance of this step, we performed a double-check of the conversion with the help of Eastman et al.'s on-line tool (available in http://astroutils.astronomy.ohio-state.edu/time/). This tool has many options to convert between time stamps, in particular, we used the first two, UTC2BJD and BJD2UTC, to make the conversions. The Eastman et al. [2010] formalism uses the following formula to convert between time stamps, adding several corrections Δ to the UTC-based Julian date:

$$BJD_{TDB} = JD_{UTC} + \Delta_{R\odot} + \Delta_C + \Delta_{S\odot} + \Delta_{E\odot}, \tag{2.1}$$

where $\Delta_{R\odot}$ is the Rømer delay, which refers to the delay or early arrival of the light from an extraterrestrial object due to the finite speed of light and the Earth traveling in its orbit. It is calculated as

$$\Delta_{R\odot} = \frac{\vec{r} \cdot \hat{n}}{c}, \tag{2.2}$$

where $\vec{r}$ is a vector from the origin of an inertial reference frame to the observer and $\hat{n}$ is the unit vector from the observer to the object, which can be written as

$$\hat{n} = \begin{pmatrix} \cos(\delta)\cos(\alpha) \\ \cos(\delta)\sin(\alpha) \\ \sin(\delta) \end{pmatrix}, \tag{2.3}$$

where α and δ are the equatorial coordinates of the object (called right ascension and declination, respectively).

The term Δ_C is the clock correction and it depends on which time standard is being used and to which is it desired to convert, if we measure time in UTC for example, the clock correction, from UTC to TDB, would be

$$\Delta_C = N + 32.184s + (TDB - TT), \tag{2.4}$$

where N is the current number of leap seconds, TT is the Terrestrial Time and 32.184s is the offset of the TT from atomic clocks (see Eastman et al.'s paper for a detailed definition of this time standards).

The term $\Delta_{S\odot}$ is the Shapiro delay, which is a general relativistic effect measuring how light passing near a massive object is delayed, it is given by

$$\Delta_{S\odot} = \frac{2GM_\odot}{c^3} \log(1 - \cos\theta), \tag{2.5}$$

where θ is the angle from the center of the Sun to the object.

Finally, $\Delta_{E\odot}$ is the Einstein delay, which is another relativistic correction needed due to the fact that the motion of the observer influences the rate at which the observed clock ticks, and it can be calculated by

$$\Delta_{E\odot} = \frac{\vec{r}_0 \cdot \vec{v}_\oplus}{c^2}, \tag{2.6}$$

where $\vec{r}_0$ is the location of the observer with respect to the geocenter and $\vec{v}_\oplus$ is the velocity of the geocenter. For our purposes, $\Delta_{R\odot}$ and Δ_C completely dominate the correction, thus $\Delta_{S\odot}$ and $\Delta_{E\odot}$ can be safely neglected.

By performing this double-check, we confirmed that the conversion with `VARTOOLS` was properly done. As a next step, we truncated the BJD_{TDB} by removing the first two digits ("24") of each of them, in order to reduce the risk of loosing numerical precision with the light curve fitting code in the next step.

In addition to our data described in Section 2.2, this time correction was also applied to the literature timings from the South African Astronomical Observatory (SAAO), Wood et al.

[1993], Lee et al. [2009], the Federal German Group for Variable Stars (BAV), the Variable Stars Network (VSNET), the American Association of Variable Star Observers (AAVSO), BRNO and Beuermann et al. [2012], who in turn used timings from MONET/North. All the HJD_{UTC} and BJD_{UTC} were converted to BJD_{TDB} in order to be able to compare all these timings with our new ones as described in Chapter 3.

Chapter 3

Light Curve Fitting

In this Chapter we detail the light curve fitting process for our data. In Section 3.1 we describe the software we used to perform this task, along with the steps we followed for each dataset. Finally, in Section 3.2 we describe the *O-C* diagram and show the *O-C* for our data.

3.1 JKTEBOP

For the light curve fitting, we used the software JKTEBOP[1] [Southworth, 2012a], which is a *Fortran 77* pipeline specially developed to fit light curves of detached eclipsing binaries and retrieve the orbital and physical parameters of the system. The software allows the user to choose which parameters should be fitted and which parameters should be fixed, as well as to provide the initial values. JKTEBOP uses non-linear least-squares optimization techniques (e.g. Levenberg-Marquardt[2]) and it has different tasks to choose from, according to how the user wants the light curve to be fitted. The error analysis of the final light curve model is done with the Monte-Carlo and bootstrapping methods implemented in the software.

Our aim by using this code was to determine the best fit values of the orbital and physical parameters of the system, and in particular, to find the eclipse timings for each night, by fitting an appropriate model to our light curves.

First we performed a test to verify that JKTEBOP was properly fitting our light curves. We ran `task3` of JKTEBOP to each preliminary light curve. This task uses the Levenberg-Marquardt minimization to fit the light curve, but provides only the formal errors from

[1] http://www.astro.keele.ac.uk/jkt/codes/jktebop.html

[2] The Levenberg-Marquardt algorithm, also known as the damped least-squares method, is used to solve non-linear least-squares problems. It is a curve fitting method that combines the Gauss-Newton and the gradient descent methods. For more information about these methods see http://people.duke.edu/~hpgavin/ce281/lm.pdf.

the covariance matrix computed by the algorithm, therefore the output uncertainties are usually underestimated. To get reliable errors even in the presence of correlated noise, we rescaled the error bars of the individual data points by multiplying them by the square root of the reduced chi squared ($\sqrt[2]{\chi^2_\nu}$). The next step was to remove the outliers from our noisiest light curves. We did this by using `task4` of `JKTEBOP`, which finds the best fit, then uses an iterative sigma-clipping algorithm to remove the outliers, and refits the data. After this preliminary steps, we proceeded to obtain a set of accurate values for the system's parameters for each individual light curve.

3.1.1 Orbital and physical parameters

The main orbital and physical parameters in an eclipsing binary system are analogous to the parameters that can be retrieved from planetary transits. In the following we will briefly describe the parameters used by the `JKTEBOP` code to fit the light curves.

Sum of the fractional radii: of the primary (R_1/a) and secondary (R_2/a) stars. It is only weakly correlated to the shape of the light curve, which leads to a better-behaved solution [Southworth, 2008].

Ratio of the radii k: between the primary and secondary stars (R_1/R_2). Like the sum of the radii, this quantity is also weakly correlated with the other parameters for a wide variety of light curve shapes, also improving the conversion to a solution.

Orbital inclination i: strongly correlated with the eclipse duration, defined as the difference between the ingress (beginning) and egress (end) times of the eclipses.

Surface brightness ratio J: the quotient between the flux density emitted at the photosphere of the primary and secondary stars.

Limb Darkening coefficients (LD): the stellar disk is brighter at the center compared to the limb of the disk, as a consequence of variations in temperature and opacity due to the depth in the stellar photosphere. We fitted a linear law for the primary star's limb darkening, and for the secondary star's limb darkening we parametrized it as a quadratic law in the cases where we had only one eclipse, therefore in these cases, two parameters are fitted, linear (μ_1) and quadratic (μ_2) [Howarth, 2011].

Reflection coefficient: a measure of the reemission of light by the hemisphere of the star facing an intense radiation field, e.g. for HW Vir the primary star is much hotter than the secondary star, therefore the reflection coefficient of the secondary star is different from zero.

Light scale factor: a normalization factor which refers to the value of the flux "out of transit", this parameter is different for each light curve, as it depends on the filter and on the data reduction process.

Eclipse time T_0: the time in BJD_{TDB} at mid-eclipse, this quantity is also different for each light curve and crucial for our analysis since it is used to calculate any variations in the period of the binary.

Since our final aim is just to get a reliable measurement of the T_0, and since it can be biased by the value of some parameters (e.g. radius of the stars, limb darkening, reflection coefficients, among others), we considered that it was better to build consistent templates of the parameters for each of the filters of our observations, to leave only T_0 as a free parameter in the final fit.

To do this, we joined all the full-phase light curves from the same filter together and left the following parameters free to find the best fit values: the sum of the radii, the ratio of the radii, the inclination, the surface brightness and the limb darkening of the primary star, the reflection coefficient of the secondary star, the scale factor and the eclipse time (T_0). We did this for the V and r filters, and additionally, for the WASP light curves.

Then we used `task9` of `JKTEBOP`, which uses a *residual-shift* method to obtain the best fit. This method evaluates the best fit for the data points and shifts the residuals of the fit point-by-point through all the data, calculating a new best fit after each shift. This approach allows to have as many best fits as points in the input light curve, and it also estimates the relevance of the correlated red noise to the parameters of the fit. The output of this task were therefore three high-accuracy templates: a V template for the Copernico/V and GAS light curves; an R/r template for the Copernico/R,r and the Schmidt/R light curves; and an unfiltered template for the WASP light curves. The best fit values of the common parameters for the light curves of each filter are shown in the histograms in Fig.3.1, where the change between the values for different filters can be observed.

Once we had the templates, we ran `task9` again for each night, now fixing all the parameters to the corresponding template values except for the eclipse times or T_0s, to retrieve the T_0s for each night. The resulting timings of HW Vir are displayed in Table 3.1, we computed a total of 25 mid-eclipse timings, which increases the current number of observations by more than 10%, and adds 6 years of baseline with respect to the latest dynamical study of HW Vir [Beuermann et al., 2012]. Furthermore, we achieved an excellent average timing error for our light curves of only ~ 2.3 s.

3.2 The *O-C* diagram

O-C stands for *Observed minus Calculated*. It evaluates the discrepancy between the measure of an observable event and its predicted value.

O-C quantities in astronomy are usually of temporal matter, when studying cyclic phenomena that are subject to anomalies in the time of occurrence. Therefore the *O-C* diagram is

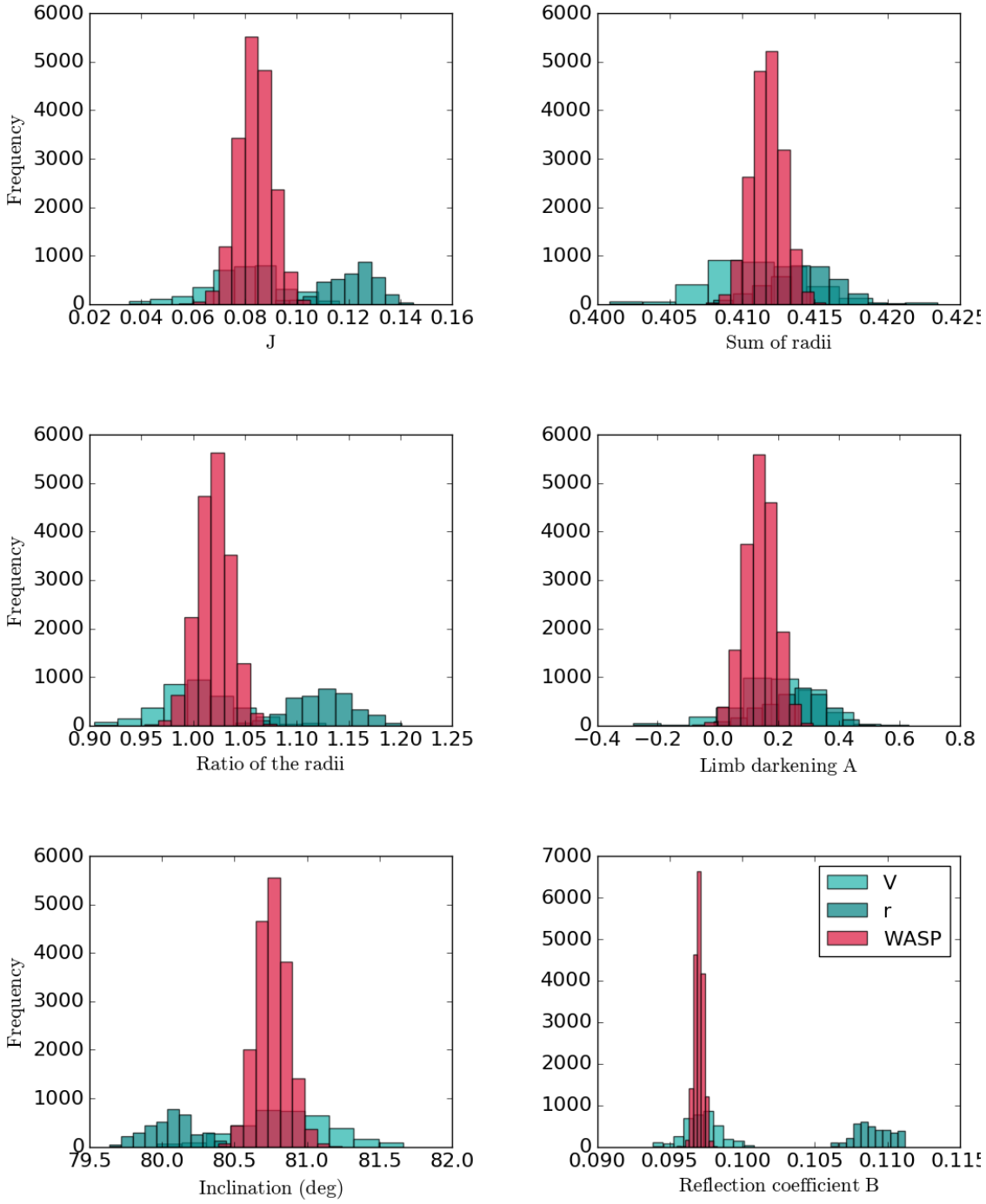

FIGURE 3.1: Histograms of the retrieved distribution of physical and orbital parameters of HW Vir from the residual-shift analysis, used to build a high-quality template of the light curve for each filter. The letters *A* and *B* indicate parameters relative to the primary and secondary star, respectively.

T_0 (BJD$_{TDB}$)	dT_0 (days)	tmed	Epoch	Origin
2455598.608756	0.000039	2455598.608749	468	Copernico
2455953.669686	0.000004	2455953.669686	3510	Copernico
2456328.572882	0.000004	2456328.572882	6722	Copernico
2456331.607585	0.000007	2456331.607585	6748	Copernico
2456723.551785	0.000006	2456723.551787	10106	Copernico
2456749.463503	0.000022	2456749.463505	10328	Copernico
2457095.536914	0.000035	2457095.536914	13293	Copernico
2457424.685857	0.000003	2457424.685856	16113	Copernico
2457427.603842	0.000006	2457427.603842	16138	Copernico
2457775.661358	0.000010	2457775.661359	19120	Copernico
2457810.560486	0.000007	2457810.560486	19419	Copernico
2457815.579418	0.000009	2457815.579417	19462	Copernico
2455998.606687	0.000022	2455998.606691	3895	Schmidt
2455999.657099	0.000048	2455999.657099	3904	Schmidt
2458229.466702	0.000026	2458229.466702	23008	Schmidt
2456729.504448	0.000022	2456729.504449	10157	GAS
2456745.495025	0.000015	2456745.495023	10294	GAS
2456746.428763	0.000023	2456746.428759	10302	GAS
2456747.479294	0.000050	2456747.479294	10311	GAS
2456748.413045	0.000025	2456748.413043	10319	GAS
2456802.454163	0.000046	2456802.454154	10782	GAS
2454539.612655	0.000012	2454539.612655	-8605	WASP
2454961.436853	0.000003	2454961.436853	-4991	WASP
2455283.582736	0.000004	2455283.582736	-2231	WASP
2455596.741284	0.000008	2455596.741284	452	WASP

TABLE 3.1: Best fit mid-eclipse times (T_0) for the primary eclipse of HW Vir along with their residuals (dT_0) and the median values (tmed) for each night. We defined the zero epoch as the number of HW Vir periods elapsed since Beuermann et al.'s reference time.

constructed by plotting the *O-C* quantity as a function of time. The *O-C* diagram can be used to study, for example, variable stars, pulsars, eclipsing systems, etc.

In order to build an *O-C* diagram to exploit the LTTE, the following concepts are needed:

An astrophysical *clock* and a long time baseline: meaning an intrinsically stable and accurate system like pulsation processes, an eclipsing system, or a pulsar, and a time baseline that is large compared to the period at which the *clock* ticks.

The Period P: defined as the time interval between successive occurrences of the same phenomena.

The Phase ϕ: the fraction of the period P that elapsed since the occurrence of the reference time T_0, and it is given by

$$\phi = \frac{T - T_0}{P} \qquad \text{modulo 1,} \tag{3.1}$$

The Linear Ephemeris: defined by

$$T_c = T_0 + PE, \tag{3.2}$$

where T_c is the calculated time of eclipse; and E is the **epoch**.

The Epoch: usually defined as the number of periods that have elapsed since the reference time T_0. In a practical sense, it can be retrieved from the observed T_0 by rounding $\frac{T-T_0}{P}$ to the nearest integer.

3.2.1 *O-C* diagram of HW Vir

In our particular case, the precise clock is the primary eclipse of HW Vir, our *observed* quantities are the eclipse timings obtained with the light curve fitting as described in Section 3.1, and the *calculated* quantities were computed using Eq. 3.2.

The *O-C* diagram for HW Vir built with our data is shown in Fig.3.2, where we plotted the *O-C* eclipse timings as a function of the epoch E, using Beuermann et al.'s ephemeris formula

$$T_c = 2445730.55018 + 0.11671 * E. \tag{3.3}$$

It can be noticed how the data from different telescopes fits remarkably well between within the error bars, which serves as a double check for both the data reduction and the time conversion.

For comparison, in Fig. 3.3 we plotted the *O-C* diagram using the literature data as well as our eclipse timings, as it can be seen, the agreement between the last literature points and our oldest values is good within the error bars, which served as a second test for the "goodness" of our data.

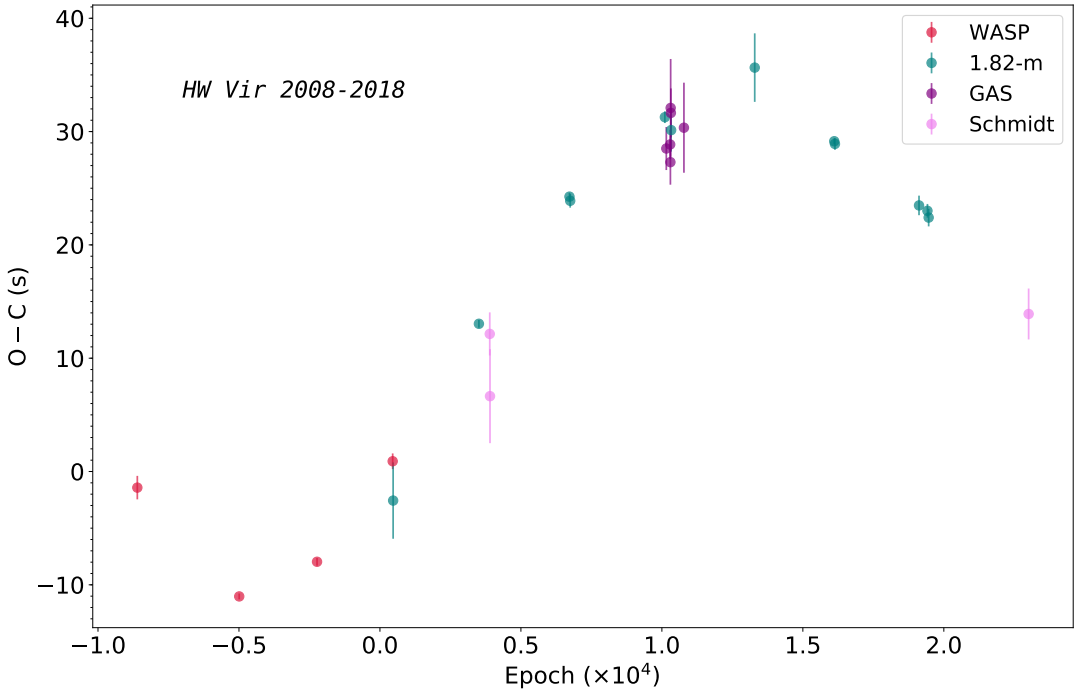

FIGURE 3.2: Observed-calculated T_0 diagram of HW Vir built with our data and the observed eclipse times obtained from the best fit of the JKTEBOP code. Some error bars are well within the size of the points.

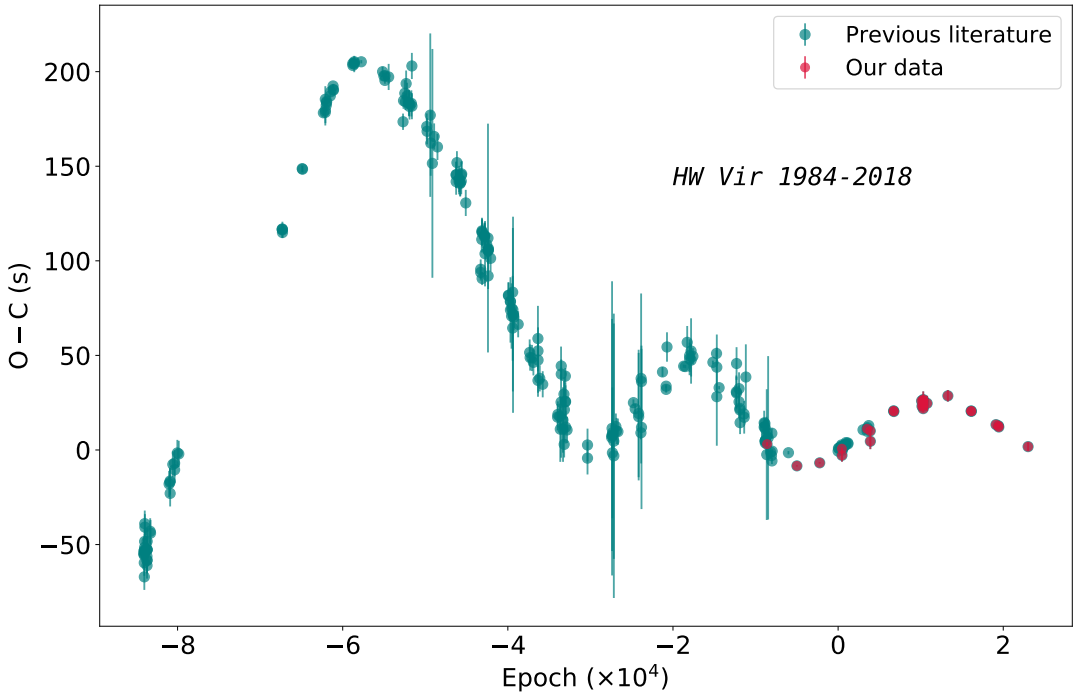

FIGURE 3.3: Observed-calculated T_0 diagram of HW Vir built with the literature data plus our data.

Chapter 4

Dynamical Modeling

In this chapter we start describing the Light Time Travel Effect (LTTE) model in Section 4.1; then in Section 4.2 we describe the software we used to reproduce the previous literature model for HW Vir and its proposed companions and we compare it with our new data; in Section 4.3 we describe the code we used to attempt to find a new solution for the system; and finally, in Section 4.4 we discuss the dynamical stability analysis of both the previous model, and of our new solutions for HW Vir.

4.1 *LTTE* calculation

First of all, we needed to calculate the LTTE (see Section 1.1.1) due to the presence of additional bodies in the system. For this purpose, we developed a *Fortran 77* code that implements an adaptation of the formula by Irwin [1952] to compute the LTTE:

$$\tau_k = K_k \left[\frac{1-e_k^2}{1+e_k \cos \nu_k} \sin(\nu_k + \omega_k) + e_k \sin \omega_k \right] \quad , \tag{4.1}$$

where the subindex $k = 1, 2, \ldots$ indicates the stellar or substellar companion causing the modulation, τ_k is the light-time delay, e_k is the eccentricity of the orbit, ω_k is the argument of periastron[1], ν_k is the true anomaly[2], and K_k is the semi-amplitude of the modulation given by

$$K_k = \frac{a_k \sin i_k}{c} \quad , \tag{4.2}$$

[1]The argument of periastron ω is the angle between the line of nodes (i.e. the intersection between the orbital plane and the reference plane) and the periastron position.

[2]The true anomaly ν is the angle between the periastron direction and the current position of the body orbiting the system.

where a_k is the semi-major axis of the orbit of the binary around the common center of mass, i_k is the inclination of the orbit with respect to the line of sight, and c is the speed of light. As a reference for the reader, the orbital elements mentioned above are illustrated in Fig. 4.1.

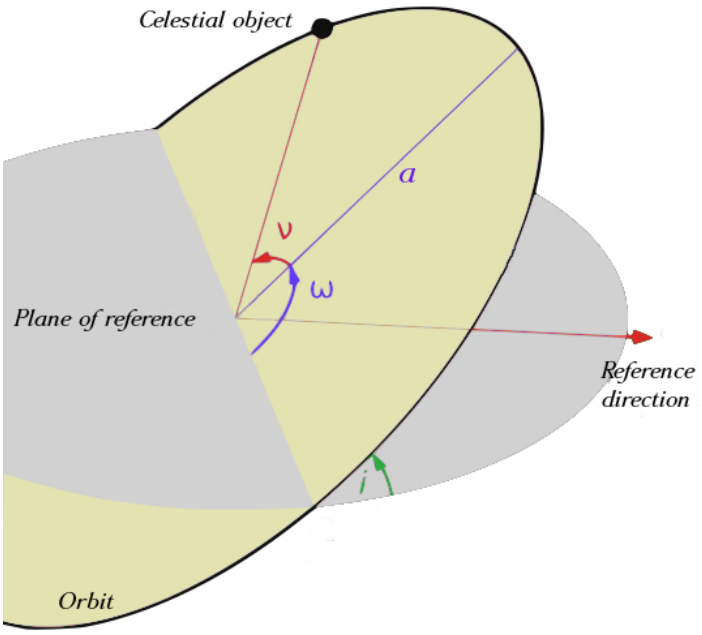

FIGURE 4.1: Orbital elements of a third body orbiting a binary system. Where i is the orbital inclination with respect to the plane of reference (or plane of the sky); a is the semi-major axis of the orbit; ω is the argument of the periastron; and ν is the true anomaly. Figure inspired in Fig. App. A.1 of Rogers [2008].

Irwin [1952] approach was to use as a the reference frame, the plane perpendicular to the line of sight that passes through the center of the elliptical orbit of the binary about the center of mass of all the bodies in the system, while our approach was to use another perpendicular (and parallel) plane to the line of sight that passes through the center of mass of all the bodies in the system as the reference frame. This approach results in the exclusion of the $e_k \sin \omega_k$ term, thus giving the following formula,

$$\tau_k = K_k \left[\frac{1 - e_k^2}{1 + e_k \cos \nu_k} \sin(\nu_k + \omega_k) \right]. \tag{4.3}$$

Notice that the shape of the light-time-curve resulting from Eq. 4.3 resembles the shape of the radial velocity-curve having half the eccentricity e and $\omega - 90°$. The velocity-curve is derived from

$$v_{rv} = K_{rv}[\cos(\omega + \nu) + e \cos \omega] \quad , \tag{4.4}$$

where the K_{rv} is the radial velocity semi-amplitude, given by

$$K_{rv} = \frac{2\pi}{P} \frac{a_* \sin i}{(1-e^2)^{1/2}} \quad , \tag{4.5}$$

with a_* the semi-major axis of the stellar orbit around the barycenter of the system.

4.2 Test of the literature model

As described in Section 1.3.1, the most recent literature model for HW Vir is the one from Beuermann et al. [2012]; who proposed a linear ephemeris plus two companions (i.e. two LTTE terms) orbiting the binary. Their best fit parameters for this two-companion model of HW Vir are displayed below in Table 4.1.

Parameter	Inner companion	Outer companion
Orbital period P (yr)	12.7 ± 0.2	55 (fixed)
Eccentricity e	0.40 ± 0.10	0.05*
Semi-major axis a (AU)	4.69 ± 0.06	12.8 ± 0.2
Mass $M \sin i$ (M_{Jup})	14.3 ± 1.0	65.0 ± 15.0
Argument of periastron ω (deg)	-18.0 ± 10.0	0.0*
Periastron passage (JD)	2452401	2461677

TABLE 4.1: Beuermann et al. [2012] parameters for the two-companion model of HW Vir. The parameters marked with * indicate "uncertain values" according to the authors.

We first wanted to reproduce the previous model prior to test it with our new data. In order to do so, we used the *Fortran 77* code mentioned in Section 4.1, which performs the calculation of the linear ephemeris as well as the contribution of the LTTE τ terms to the *O-C* diagram using Eq. 4.3. The software takes the orbital parameters of the system (depicted in Fig. 4.1) as an input and provides three output files: the first one includes the linear ephemeris with their errors; the second one contains the full *O-C* model, which includes the linear ephemeris, as well as the τ_3 and τ_4 contributions from the proposed companions; and the third one only displays the *O-C* model, in order to make it easier to plot the solutions, allowing a better comparison.

We ran the code using Beuermann et al.'s parameters along with their data, in order to reproduce their model. This served also as a double-check that the software was working properly. The results for this test are displayed in Fig. 4.2, where we see that our code is able to reproduce the literature model remarkably.

Then, we used both all the available literature timings along with our new data, giving our timings zero weight so that the model would not be affected by them and we would be able to measure the fit of the model to our values. We display our results in Fig. 4.3. From this

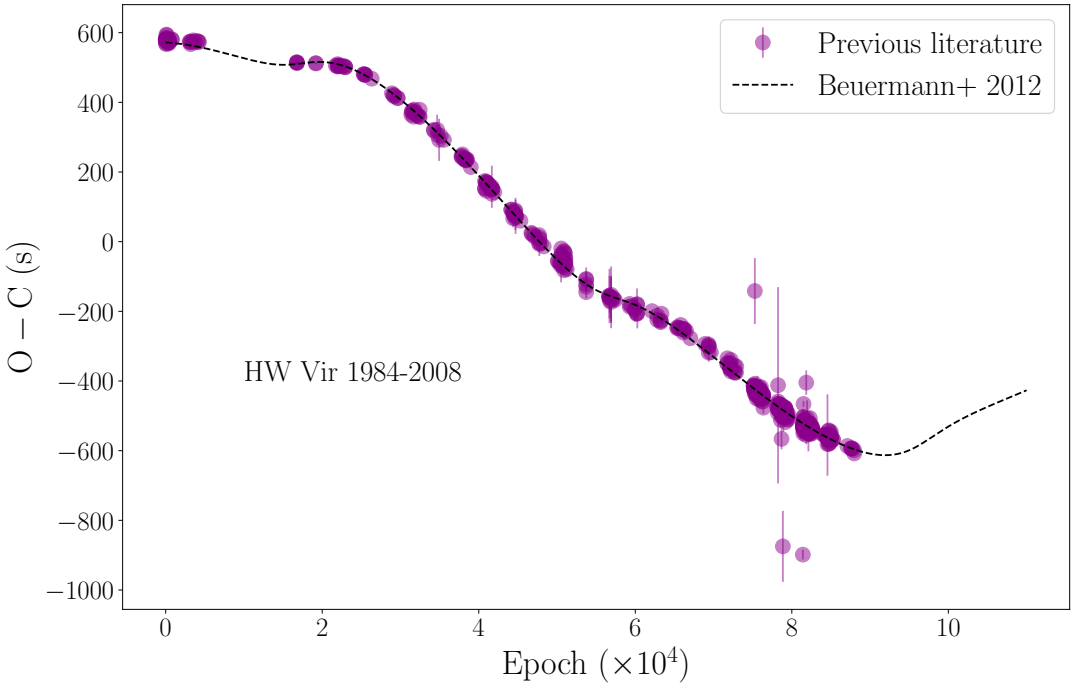

FIGURE 4.2: *O-C* diagram of HW Vir showing Beuermann et al.'s model along with all the literature timings available. The model fits the data perfectly within error bars. Some of which fall well within the size of the points.

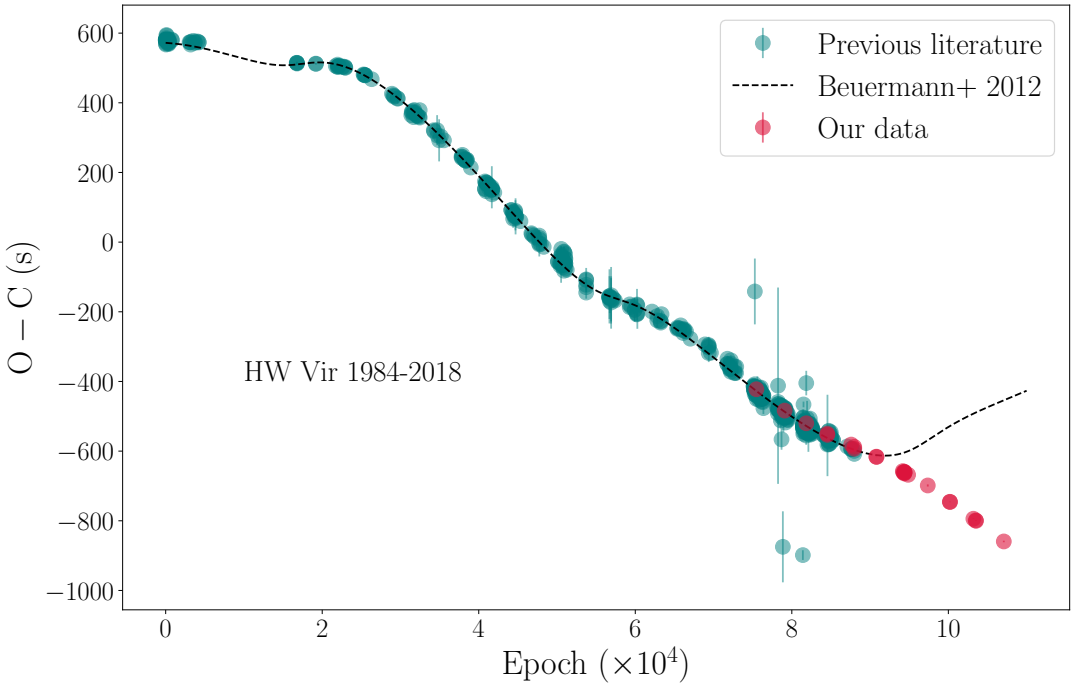

FIGURE 4.3: The same *O-C* diagram of HW Vir as in Fig. 4.2, with the model extended along time and our new timings over-plotted for comparison. It is clear that Beuermann et al.'s model fails to describe our data. Some of the error bars fall within the size of the points.

plot, we see that Beuermann et al.'s model is able to fit the data up to 2012, but after that it fails to reproduce our new timings. The discrepancy we find is completely out of the error bars, disproving the previous model.

4.3 The search for a new model

Given the results of the previous Section, the next logical step is to propose a new model that is able to fit both the old and new observations.

As a first step, we wanted to explore all the parameter space for the two-companion model for HW Vir. Before we attempted to find a new model that fits the observations, we discarded the first two seasons from the literature, since their errors may have been underestimated and they correspond to very old observations ($\sim$ 1980). We also rescaled all the T_0 errors by adding in quadrature 1 s to Beuermann et al.'s and our values, and 5 s to the rest of the literature values; this to take into account realistic absolute calibration uncertainties and make sure that we were not underestimating the errors. After removing the outliers and rescaling the errors, we used a *Fortran 77* code based on the software described in Section 4.2 but improved with the implementation of the `PIKAIA` subroutine, which uses a genetic algorithm to solve multi-modal optimization problems, such as finding the best set of parameters for HW Vir and its companions.

Genetic algorithms

Genetic algorithms (hereafter GAs) are a family of adaptive search methods based on the theory of biological evolution, driven by natural selection, which starts with the election of the fittest individuals from a population. These individuals then breed producing offspring which inherit the *genes* (characteristics) from their parents. If the parents have a higher fitness, their offspring will be better than them and will have more chances to survive and breed again. As a result, the new generation will always have a higher fitness than the previous one.

In practice, GAs start with an *initial population*, composed by *individuals* (solutions) each consisting in a set of parameters randomly generated from the entire range of all possible model parameters (i.e. the phase space). A *fitness function* is required to determine how "fit" an individual of the population is. It assigns a fitness score to each individual, and this score determines the probability that an individual will be selected for reproduction [Charbonneau, 1995]. A common example of a fitness function is the inverse of the chi-square χ^2.

GAs work in the following manner:

1. The *goodness of fit* of each member of the population is evaluated.

2. The *selection* of pairs of solutions from the current population that will reproduce passing their characteristics to their offspring takes place.

3. The new pair of offspring is produced according to the *crossover* rules, which establish which parameters will be exchanged among the parents to produce the offspring.

4. Optionally, *mutation* can occur in a certain number of the parameters from the produced offspring, with a low random probability.

5. Steps 2. to 4. are repeated until the population of offspring is as large as the initial population.

During all the process, the population maintains a fixed size, as new generations are formed, the individuals with the lowest fitness score are discarded, providing space for new offspring. The algorithm should be in principle, stopped when the population converges to a solution, i.e. when it does not produce offspring that is significantly different from the previous generation. This can be determined only by the fitness function [Charbonneau, 1995].

GAs are preferred by many over other techniques (such as artificial intelligence techniques, for example) since they are more robust to changes in the inputs, or in the presence of a certain level of noise [Williams and Guidry, 2004].

4.3.1 The `PIKAIA` subroutine

The `PIKAIA` subroutine[3] (written by Charbonneau [1995]) features two basic genetic algorithm operators, the *uniform one-point crossover*, and the *uniform one-point mutation*. There are three reproduction plans available: "full generation replacement", "Steady-State-Delete-Random", and "Steady-State-Delete-Worst". It is also possible to choose "*elitism*"[4] and it is implemented by default. The selection process is based on the fitness ranking and performed in a stochastic way, using the Roulette Wheel Algorithm[5]. The code has a ranking subroutine based on the Quicksort Algorithm [Fouz et al., 2009], and generates random numbers based on a minimal standard Lehmer generator. The user can control the mutation rate based on the difference between the best and median fitness values of the current population.

The code can run under two different modalities: the user can choose between generating the initial population in a random way providing boundaries for each parameter to be "evolved"; or to provide an initial population.

For our purposes, we used the first modality of `PIKAIA` and for the boundaries we considered a wide range from Beuermann et al.'s parameters (shown in Table 4.2), this because from

[3] `http://www.hao.ucar.edu/modeling/pikaia/pikaia.php`

[4] Elitism implies copying the fittest solutions of the current generation, unchanged, to the next generation.

[5] The Roulette Wheel Algorithm is used to select an individual proportional to its probability, which is assigned based on the individual's fitness level.

Parameter	Minimum value	Maximum value
T_0 (BJD$_{TDB}$)	2445730.0	2445731.0
P (days)	0.11671	0.11673
T_3 (days)	2452000.0	2459000.0
T_4 (days)	2461000.0	2491000.0
e_3	0.0	0.5
e_4	0.0	0.7
P_3 (days)	2000.0	7000.0
P_4 (days)	10000.0	30000.0
$a_3 \sin i$ (AU)	0.0	30.0
$a_4 \sin i$ (AU)	0.5	50.0
ω_3 (deg)	0.0	360.0
ω_4 (deg)	0.0	360.0

TABLE 4.2: Parameter boundaries for HW Vir and its proposed companions, used as an input for the PIKAIA code. The subscripts 3 and 4 refer to the inner and outer companions, respectively.

Fig. 4.3 it is seen that their model is not completely far off the actual one, but we took the precaution of keeping the boundaries wide enough to cover several other possibilities in the phase space.

We performed 100,000 simulations of 1000 generations each on a population of 200 individuals and we used the inverse of the chi-square $1/\chi^2$ as our fitness function.

Once the code computes the results for PIKAIA at the end of each simulation, it uses the Levenberg-Marquardt (LM) algorithm to calculate the final best-fit solution, using as input, the PIKAIA output. The LM algorithm uses the reduced chi square χ^2_ν as the function to be minimized (that is, as a least-square approach). However, it does not take into account any boundaries for the parameters, therefore, the final results from the code can be even unphysical. To end up only with physically meaningful solutions, we selected only the sets of solutions for which the parameters are within the initial boundaries (see Table 4.2) and have a χ^2_ν between 0 and 10, the latter for visualization purposes.

The results of the simulations are displayed in the following figures. In Fig. 4.4 we compare the results for the T_0 vs the orbital period of HW Vir; for the companions, we compared the times of periastron passage (Fig. 4.5), the eccentricities (Fig. 4.6), the orbital periods (Fig. 4.7), the semi-major axes relative to the barycenter of the system (Fig. 4.8), and the arguments of periastron (Fig. 4.9). With these comparison plots, showing 2-D slices of our 12-parameter solution space, we were able to find the "sweet spots" with the best χ^2_ν, which intersection give us the parameter vectors that are the best solutions for the LTTE of HW Vir.

In Fig. 4.10 we plotted the *O-C* diagram for the two-companion model corresponding to the best solution (lowest χ^2_ν) of the PIKAIA+LM code. In the central panels, we plotted the individual contributions from the inner and outer companions, τ_3 and τ_4, respectively. As well as the residuals after the subtraction of the contributions by the two companions. From

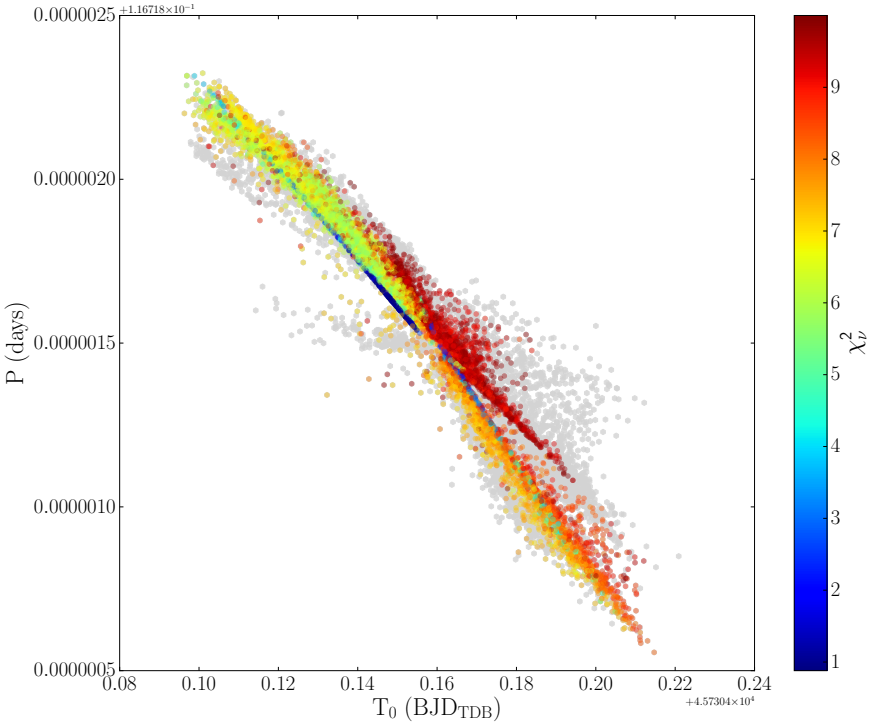

FIGURE 4.4: HW Vir T_0 vs its orbital period P.

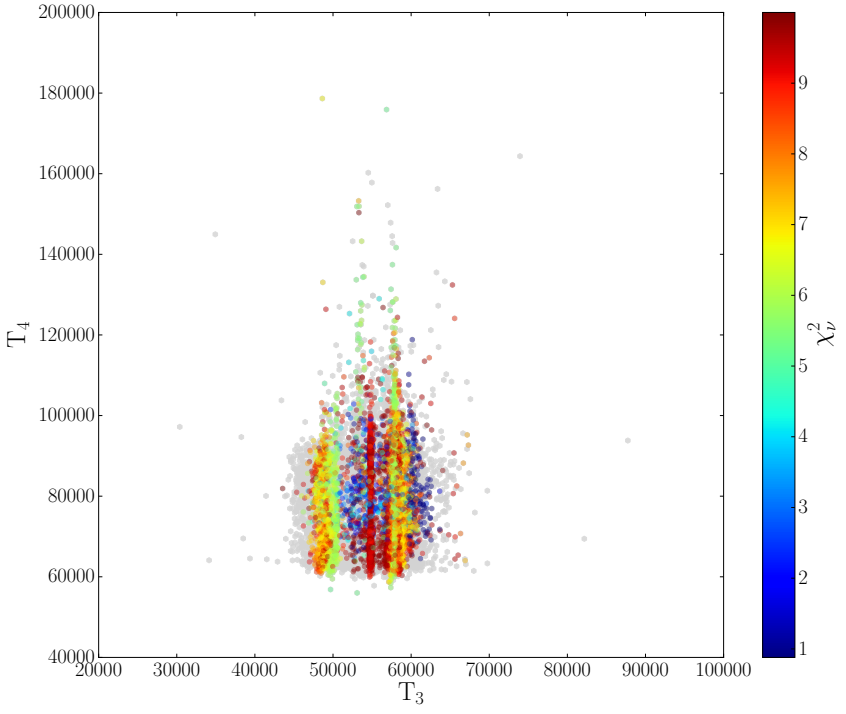

FIGURE 4.5: Times of periastron passage in BJD_{TDB} - 2400000 days of the proposed two companions for HW Vir.

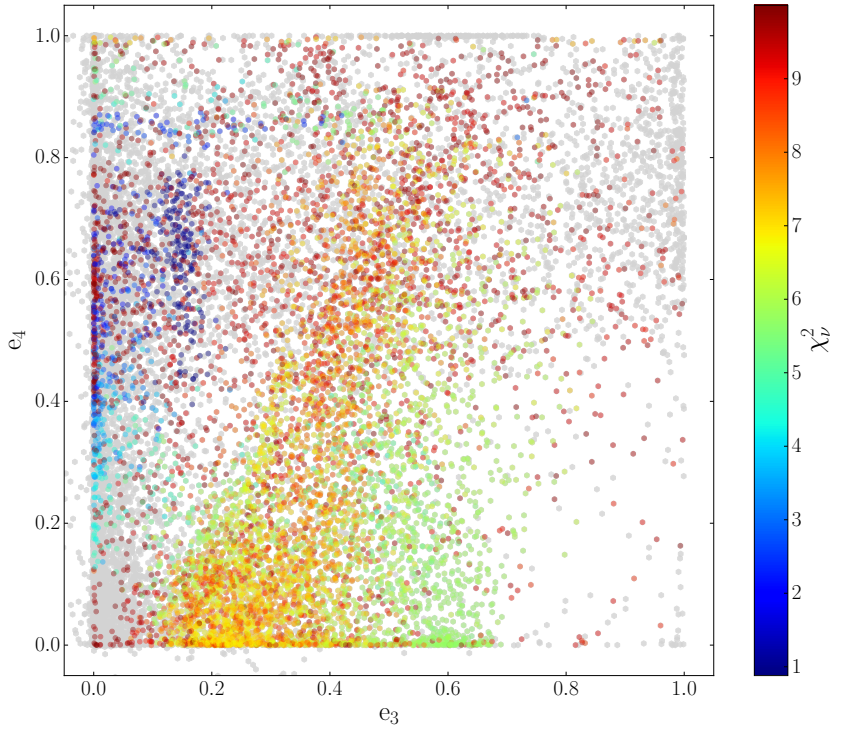

FIGURE 4.6: Eccentricities of the two proposed companions of HW Vir. In this case the LM algorithm leaded to unphysical values ($e < 0$) as can be seen in this plot.

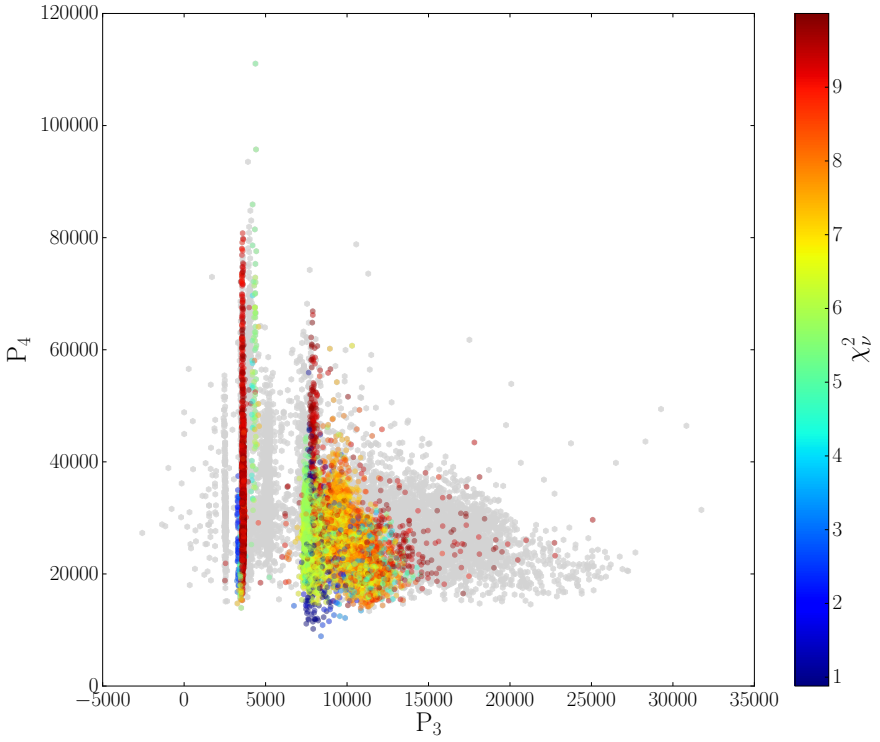

FIGURE 4.7: Orbital periods in days of the proposed companions of HW Vir. As it can be seen, some values are negative (and thus, unphysical), resulting from the LM algorithm.

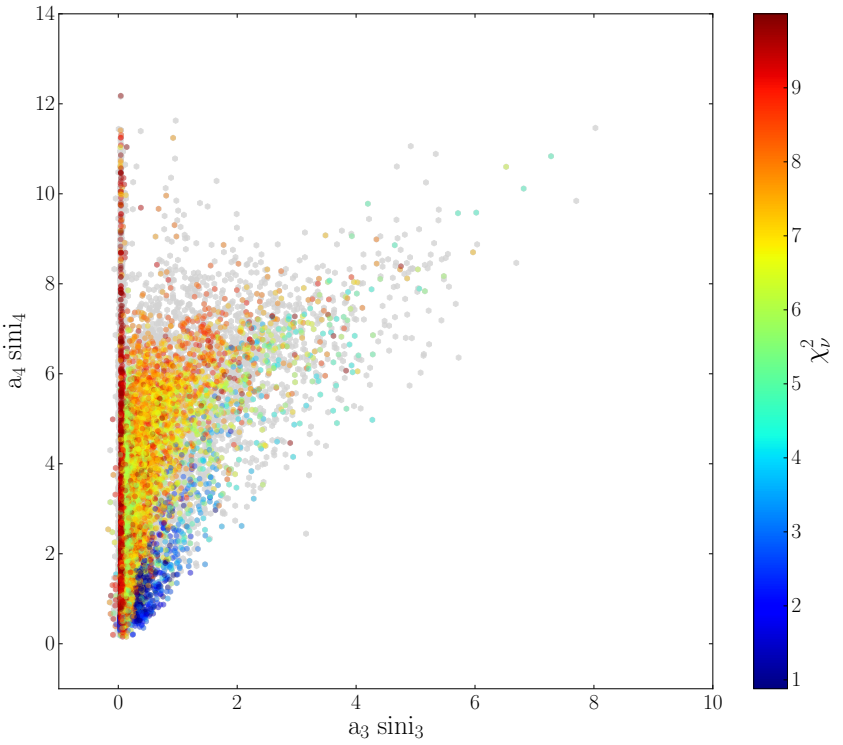

FIGURE 4.8: Semi-major axes in *AU* of the companions of HW Vir relative to the barycenter of the system taking into account all the bodies in it. Again, we see that there are some unphysical values, resulting from the LM algorithm.

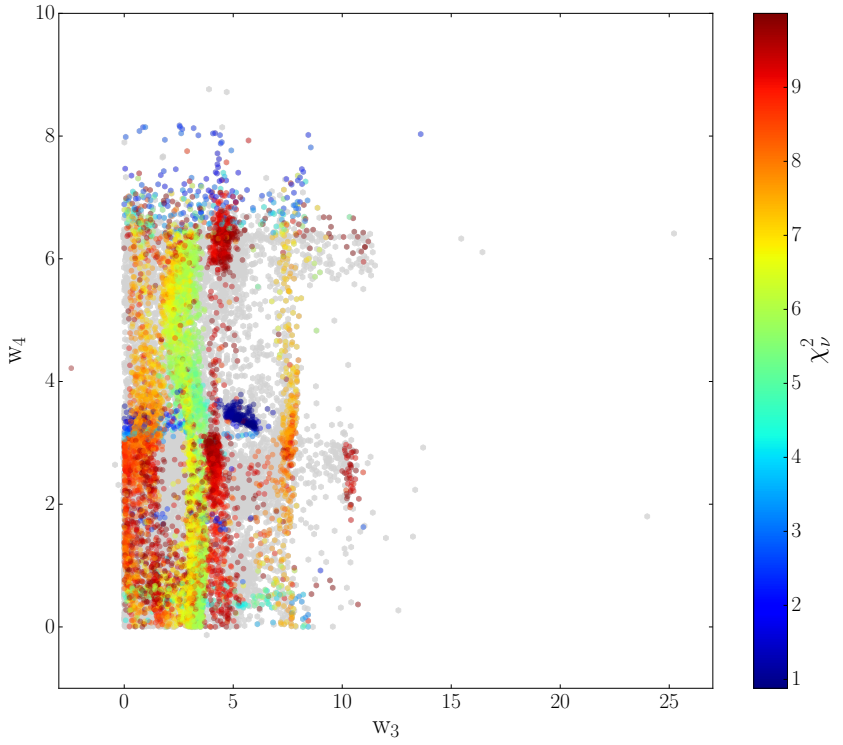

FIGURE 4.9: Argument of periastron in deg of the proposed companions of HW Vir. The LM algorithm leaded to unphysical values in this case as well.

this plots we see that the model is in excellent agreement with all data and it is able to fit it remarkably.

To test the dynamical stability of the systems resulting from our new sets of parameters, we selected only the solutions that fulfilled the conditions of both being physically feasible in a broader sense, that is within the initial PIKAIA boundaries shown in Table 4.2; and that had χ^2_ν between 0.5 and 1.5. Then we calculated the mass and the semi-major axis of each of the companions of HW Vir. To do this, we used the following relation from the two-body problem:

$$a_{kbar} = a_k \frac{m_k}{M_{bin} + m_k} \quad , \tag{4.6}$$

where $a_{kbar} \sin i$ is the semi-major axis relative to the barycenter of the system (the one retrieved by PIKAIA), M_{bin} is the sum of the masses of the binary, m_k is the mass of the k-th companion of HW Vir, and a_k is the semi-major axis, which we substituted from Kepler's third law:

$$P_k^2 = \frac{4\pi^2 a_k^3}{G(M_{bin} + m_k)} \quad , \tag{4.7}$$

where P_k is the period of each companion. After substituting and rearranging the terms, we calculated the minimum mass of each companion ($m_k \sin i$) using

$$m_k \sin i = \left[\frac{4\pi^2 (a_{kbar} \sin i)^3 M_{bin}^2}{G P_k^2} \right]^{1/3} , \tag{4.8}$$

where i is the inclination of the orbit of each companion. After computing the mass, we retrieved the semi-major axis a_k from Eq. 4.6.

The results for these calculations are shown in the histograms of Fig. 4.11, Fig. 4.12 for the masses, and in Fig. 4.13 and Fig. 4.14 for the semi-major axes. For the masses, we see that the values are quite high, falling within the substellar and stellar classification, 13 M_{Jup} and 82 M_{Jup}, respectively. Where 13 M_{Jup} represents the conventional deuterium burning limit (i.e. the boundary between planets and brown dwarfs), and 82 M_{Jup} is the hydrogen burning limit (i.e. the boundary between stars and brown dwarfs). In the case of the semi-major axes, the values we find are within the values proposed by Beuermann et al.

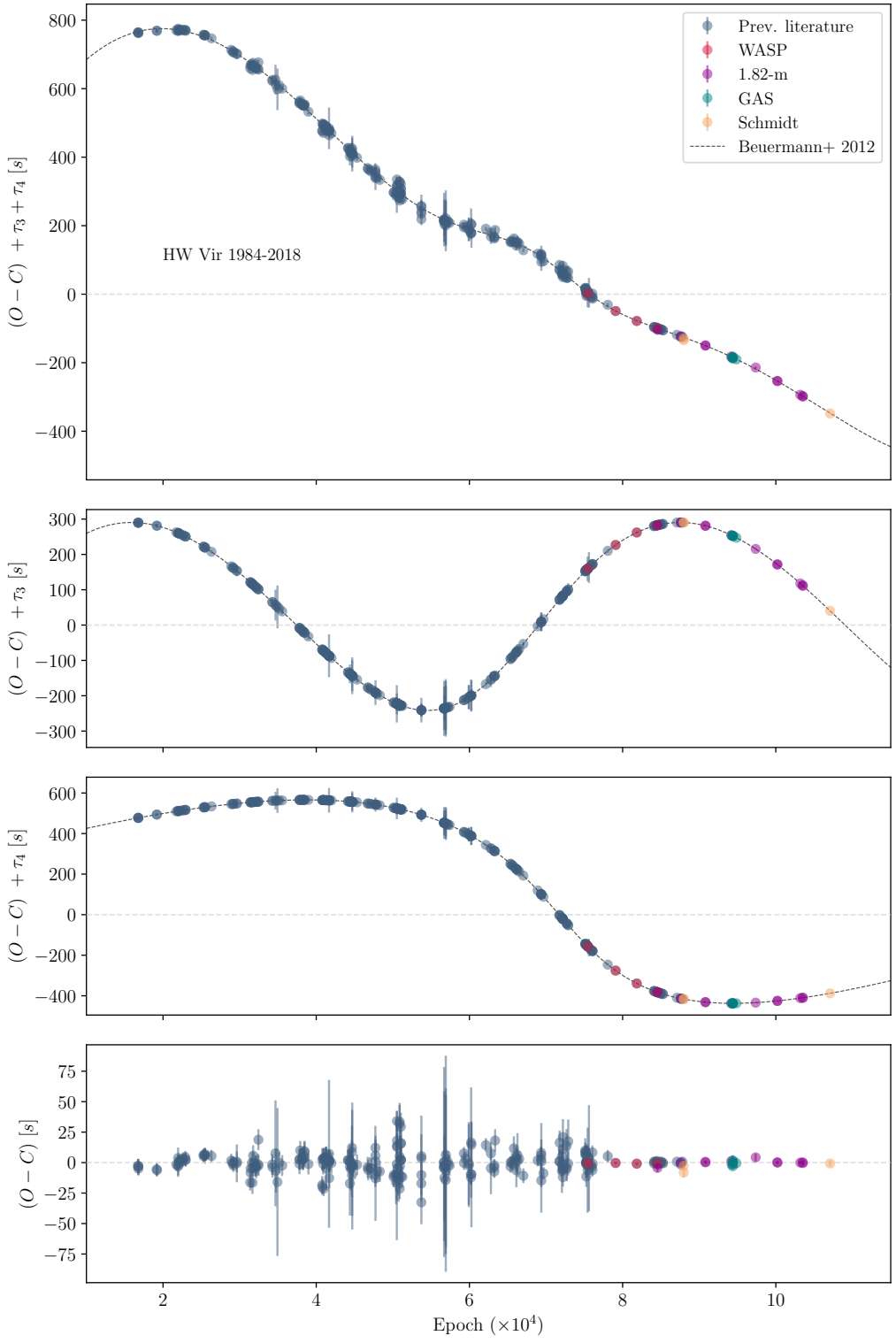

FIGURE 4.10: Two-companion model fit to all the data from the best-fit solution of the PIKAIA+LM code. *Top: O-C* plus the contribution of the two companions. *Central panels: O-C* plus the contribution of each of the companions along with their corresponding model. *Bottom:* residuals after the subtraction of the contributions by the two companions. Some of the error bars fall within the size of the markers.

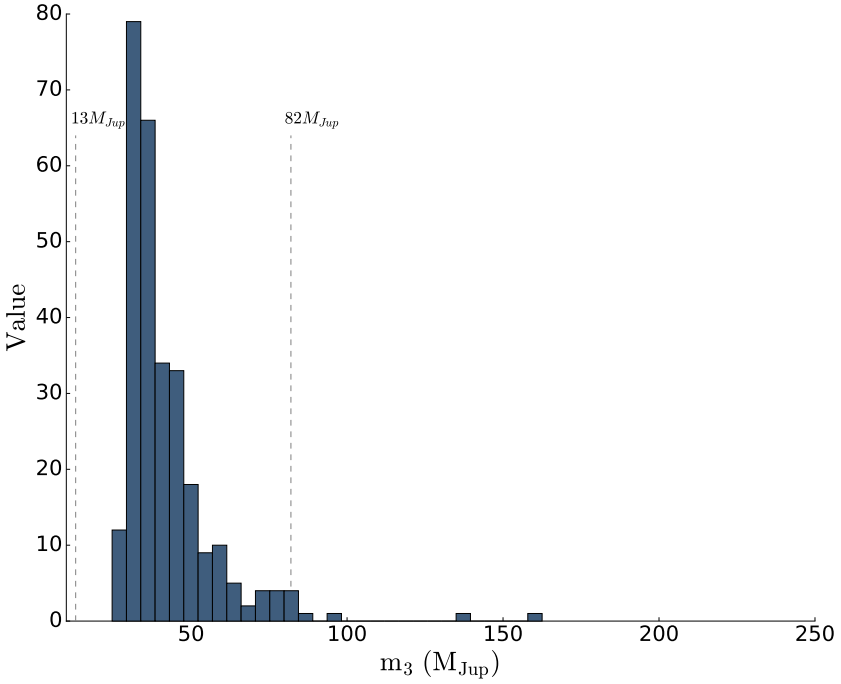

FIGURE 4.11: Histogram of the minimum mass of the inner companion of HW Vir in M_{Jup} for the best-fit solutions from PIKAIA+LM with $0.5 < \chi^2_\nu < 1.5$. The $13M_{Jup}$ and $82M_{Jup}$ lines indicate the deuterium and hydrogen burning limits, respectively (see text).

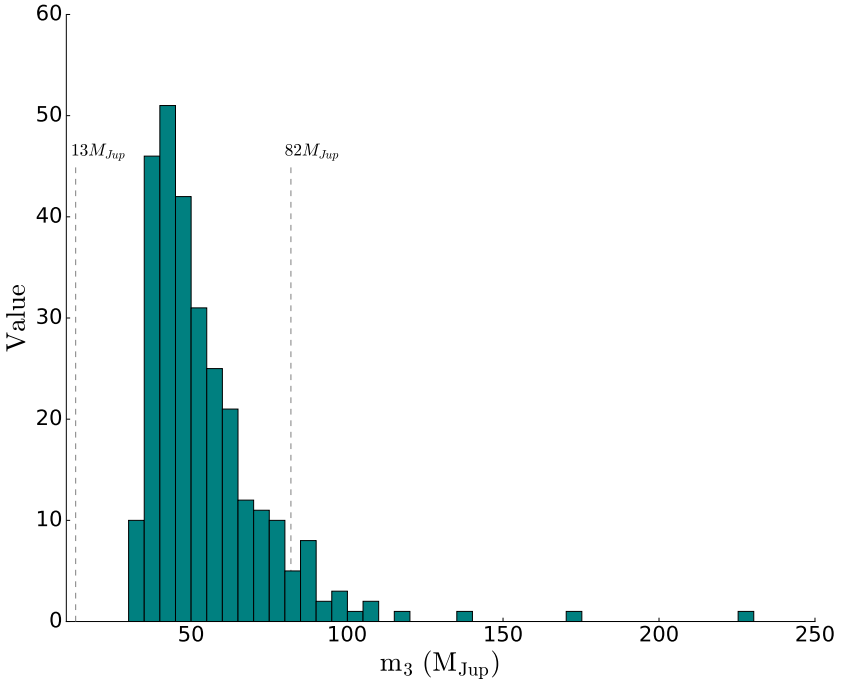

FIGURE 4.12: Histogram of the minimum mass of the outer companion of HW Vir in M_{Jup} for the best-fit solutions from PIKAIA+LM with $0.5 < \chi^2_\nu < 1.5$. The $13M_{Jup}$ and $82M_{Jup}$ lines indicate the deuterium and hydrogen burning limits, respectively (see text).

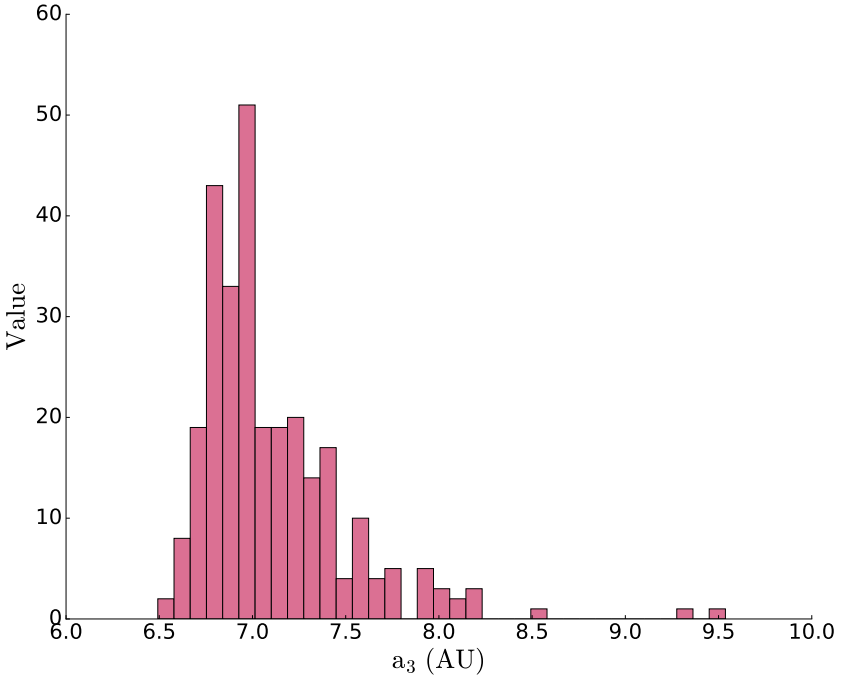

FIGURE 4.13: Histogram of the semi-major axis of the inner companion of HW Vir in *AU* for the best-fit solutions from `PIKAIA+LM` with $0.5 < \chi^2_\nu < 1.5$.

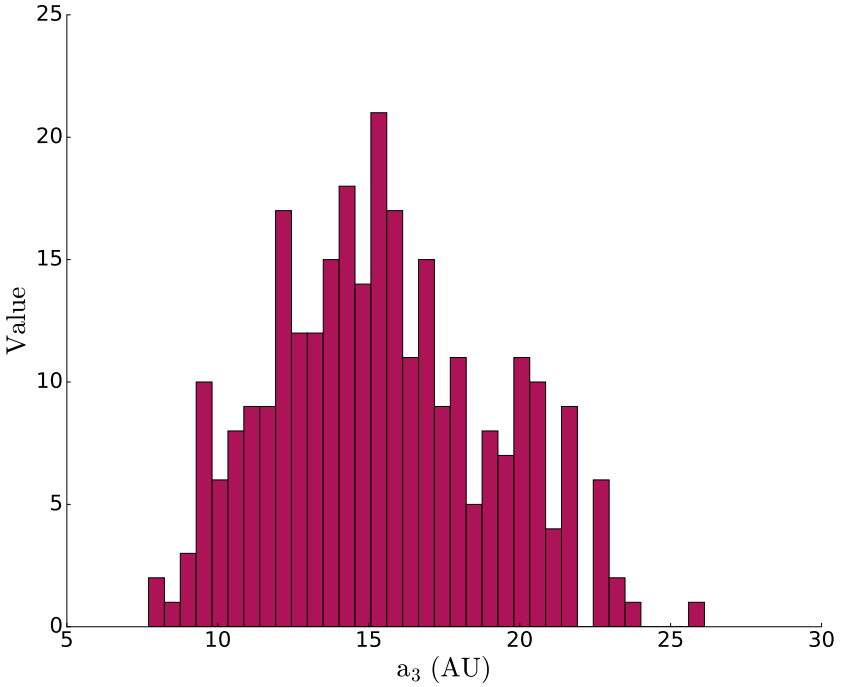

FIGURE 4.14: Histogram of the semi-major axis of the outer companion of HW Vir in *AU* for the best-fit solutions from `PIKAIA+LM` with $0.5 < \chi^2_\nu < 1.5$.

4.4 Dynamical stability

As an additional task, we tested the dynamical stability of the best-fit solutions we found in the previous Section.

4.4.1 Dynamical analysis with `Mercury6`

For this we used the code `Mercury6`, a *Fortran77* N-body integrator modified from the original version from Chambers, by I. Dovgalev (`https://github.com/4xxi/mercury`). This new version provides double precision in the calculations as well as a few modifications to the input files to make the software more user-friendly. The code performs orbital integrations for planetary systems dynamics, which allows to study the long-term stability and orbital evolution of planets and smaller bodies (such as comets or asteroids) as well as to monitor close encounters, ejections and collisions between the bodies in the system. The software includes the option to choose among different N-body integrator algorithms, from which we used both the hybrid symplectic and Everhart's RA15 (RADAU) ones as explained below. `Mercury6` allows to input initial conditions in either Cartesian or Keplerian elements in *asteroidal* or *cometary* formats. As an output, the software can provide the positions and velocities, as well as the orbital elements for each time step (determined by the user) of the integration. The first ones allow to reconstruct the orbits of the components of the system. The user can determine all the desired options for both the input and output formats in the different input files.

It is important to acknowledge that neither the original `Mercury` nor `Mercury6` are suitable to integrate close-in binaries for numerical reasons. However, we used `Mercury6` following the prescription of Beuermann et al., who considered the binary as a single central body with the mass of the two components of the binary, justifying their approach with the fact that the gravitational field of HW Vir is felt by its distant companions as a constant field created by the combined mass of the binary components plus a gravity wave, which they estimate to be negligible.

We used `Mercury6` with the hybrid symplectic integrator and Keplerian elements for the input parameters using the values retrieved from the `PIKAIA` code. To run `Mercury6`, a series of input files that contain the orbital and physical parameters of all the components of the system, as well as the code's constrains and the output format, has to be prepared. We performed the integration of a subsample of the "best-fit-physically-feasible" set in the same way as Beuermann et al., assuming the binary as a single body with mass $M_{bin} = m_1 + m_2$. As a first test, we integrated for a range of timespans from 10000 days to 10^4 yr, in order to save in computational time, as well as to test the stability in short timescales. For the integration step size, we took values around two hundredths of the period of the inner companion P_3, to check whether there were any events taking place within P_3. For the cases we tested, the

output for `Mercury6` showed that in general the orbits were not stable, and in some cases, the inner or the outer companions were expelled after a few thousand years.

With these results, we decided to try to reproduce the stability simulation of Beuermann et al.'s model. We followed their steps to the best of our knowledge, using the same integrator (hybrid symplectic) and Keplerian elements as an input with their values, as well as assuming the binary star to be a single body of $M_{bin} = m_1 + m_2$. To begin with, we integrated for 10^4 yr, and surprisingly, we found that the inner planet is ejected after $\sim$ 2500 yr, which is in disagreement with Beuermann et al.'s paper, where they claim that their proposed model is stable for 10^8 yr.

To try to understand this discrepancy, we performed some additional tests by varying the values of the parameters within the errors, but we did not arrive to a definitive explanation for this inconsistency. In any case, we did this only as a test since as we explained in Section 4.2, we found Beuermann et al.'s model to be incompatible with our data.

4.4.2 `Mercury6` for binaries

As a double-check for our new models, we tried to test the stability with a different version of `Mercury6`, `Mercury6_binary`[6], which is another modified version of `Mercury` by Smullen et al. [2016]. This version of the software allows to simulate both single and binary stars, treating the central star in the binary as a composite "big body" instead of a single central object.

We performed the stability tests of our models with the new parameters found using the `PIKAIA` code as explained in Section 4.4.1, this time with the components of the binary as two separate bodies. For the integration we used the advised RADAU integrator, regarding the integration time, we tried with a few thousand years, and we kept the step size of the integration to about one P_4 as before.

In a 100% of the tests, the orbit of the secondary star of HW Vir is well simulated; however, both the inner and outer companions are ejected after a few decades. Despite the "goodness of fit" that the solutions had, `Mercury6_binary` was unable to find a stable system even in short timescales ($< 10^4$ yr). Among the causes behind this behavior, there is the possibility that `Mercury6_binary` is not suitable to integrate close-in binaries with massive companions like HW Vir, although the program succeeds in integrating the binary system in an accurate way.

Regardless of the underlying cause for the unsuccessful stability of the system, this evidences the challenge that solving a multi-variable problem like this represents, and calls into question the previous published results.

[6] https://github.com/rsmullen/mercury6_binary

Chapter 5

Summary and Conclusions

In this thesis we presented a study of the eclipsing binary system HW Virginis by using unpublished photometric observations from four different sources; two telescopes from the Asiago Astrophysical Observatory (the 1.82-m and the Schmidt telescope), an amateur telescope from the "Gruppo Astrofili Salese Galileo Galilei", and a large dataset from the SuperWASP consortium.

During the data reduction we paid particular attention to minimize the photometric errors and to convert the light curve time into a common reference frame, as it was crucial for the purposes of this work to have an accurate time stamp and be able to compare datasets from different sources.

We performed the light curve fitting to determine the best fit values for the orbital and physical parameters of HW Vir, with this we were able to extract the eclipse timings for each night. By combining our new timings with the ones available in the literature, we found that they are in good agreement within error bars, showing that our data reduction and light curve fitting process were accurate. With these new timings, we increased the baseline of the existing observations of HW Vir by 10 years.

We reproduced the most recent literature model for HW Vir and obtained the same results as Beuermann et al.. However, we discovered that this model is unable to fit our new data, and therefore had to be revised. Additionally, we tested the dynamical stability of their proposed model and surprisingly, we found it to be unstable after only a few thousand years, when they claim it was stable for 10^8 yr.

As a first effort to find a correct model for the LTTE in HW Vir, we used the `PIKAIA` code, which implements a genetic algorithm to explore the parameter space and estimate new parameters for the companions of the binary system. We found a set of parameter vectors with a very good fit in a statistical sense, able to explain all the available data. Notwithstanding, these sets of solutions led to very high values for the masses of the companions of HW Vir ($\sim 50 M_{Jup}$, within the mass range of brown dwarfs) and unstable systems.

Despite a satisfying explanation for the ETVs of HW Vir is still eluding us, it was equally important to highlight the fact that there is still a lot to be learned about all the systems of this kind and this one in particular. One of the challenges to accurately determine the underlying cause of the ETVs in this case, is that the observations show that the period of one of the components from the LTTE of HW Vir is longer than the total observational timespan available. Therefore, increasing the observational baseline will certainly bring us closer to determine the cause behind the ETVs of HW Vir.

5.1 Future work

A possible alternative to explain HW Vir's ETVs could be a one-companion model plus a quadratic term in the ephemeris of the binary star, implying an intrinsic and constant decreasing rate of the orbital period. The `PIKAIA` code can be modified to find solutions for this kind of system, therefore a next step could be to test the feasibility of this solution.

So far, the results of this work suggest that it would be interesting to study HW Vir with other techniques, for example, using direct imaging, given the evidence that the possible companions are in such wide orbits, as well as are likely high in mass, which makes this system an excellent candidate to observe with this method.

A deeper understanding of how the Applegate mechanism actually works, will help in investigating whether the observed *O-C* signal could in part be due to an intrinsic stellar effect rather than to an LTTE modulation by additional bodies. This could be achieved by studying the (still poorly known) physical details of late-type stars with the help of missions like Gaia, and new, state-of-the-art facilities like the E-ELT.

List of Figures

1.1 Direct imaging . . . 2
1.2 Radial velocity . . . 3
1.3 Astrometry . . . 3
1.4 Microlensing . . . 4
1.5 Transits . . . 5
1.6 Timing . . . 6
1.7 HW Vir . . . 11
1.8 HW Vir O-C by Beuermann et al. . . . 12

2.1 1.82-m . . . 16
2.2 Schmidt . . . 17
2.3 SuperWASP . . . 19
2.4 182 light curves . . . 21
2.5 Schmidt light curves . . . 21
2.6 GAS light curves . . . 22
2.7 HW Vir field . . . 23
2.8 WASP light curves . . . 24

3.1 Histograms of the retrieved distribution of physical and orbital parameters of HW Vir from the residual-shift analysis . . . 30
3.2 O-C diagram of HW Vir built with our data . . . 33
3.3 O-C diagram of HW Vir with the literature values plus our data . . . 33

4.1 Orbital elements . . . 36
4.2 Beuermann's model and data . . . 38
4.3 Literature model and data with our data . . . 38
4.4 HW Virginis T_0 vs P . . . 42
4.5 Periastron passages of the two proposed companions of HW Vir . . . 42
4.6 Eccentricities of the two proposed companions of HW Vir . . . 43
4.7 Orbital periods of the companions of HW Virginis . . . 43
4.8 Semi-major axis for the companions of HW Virginis . . . 44
4.9 Argument of periastron of the companions of HW Virginis . . . 44
4.10 *O-C* diagram for the two-companion model for HW Virginis . . . 46
4.11 Histogram of the values for the minimum mass of the inner companion of HW Vir . . . 47

4.12 Histogram of the values for the minimum mass of the outer companion of HW Virginis 47
4.13 Histogram of the values for the semi-major axis of the inner companion of HW Virginis 48
4.14 Histogram of the values for the semi-major axis of the outer companion of HW Virginis 48

List of Tables

1.1 HW Vir parameters from the most recent literature 10

2.1 HW Vir observations 18

3.1 Eclipse Timings of HW Vir obtained with our data 31

4.1 Beuermann et al. parameters for the companions of HW Vir 37
4.2 Parameter boundaries of HW Vir and its proposed companions 41

Bibliography

J. H. Applegate. A mechanism for orbital period modulation in close binaries. ApJ, 385: 621–629, February 1992. doi: 10.1086/170967.

J.-P. Beaulieu, D. P. Bennett, P. Fouqué, A. Williams, M. Dominik, U. G. Jørgensen, D. Kubas, A. Cassan, C. Coutures, J. Greenhill, K. Hill, J. Menzies, P. D. Sackett, M. Albrow, S. Brillant, J. A. R. Caldwell, J. J. Calitz, K. H. Cook, E. Corrales, M. Desort, S. Dieters, D. Dominis, J. Donatowicz, M. Hoffman, S. Kane, J.-B. Marquette, R. Martin, P. Meintjes, K. Pollard, K. Sahu, C. Vinter, J. Wambsganss, K. Woller, K. Horne, I. Steele, D. M. Bramich, M. Burgdorf, C. Snodgrass, M. Bode, A. Udalski, M. K. Szymański, M. Kubiak, T. Więckowski, G. Pietrzyński, I. Soszyński, O. Szewczyk, Ł. Wyrzykowski, B. Paczyński, F. Abe, I. A. Bond, T. R. Britton, A. C. Gilmore, J. B. Hearnshaw, Y. Itow, K. Kamiya, P. M. Kilmartin, A. V. Korpela, K. Masuda, Y. Matsubara, M. Motomura, Y. Muraki, S. Nakamura, C. Okada, K. Ohnishi, N. J. Rattenbury, T. Sako, S. Sato, M. Sasaki, T. Sekiguchi, D. J. Sullivan, P. J. Tristram, P. C. M. Yock, and T. Yoshioka. Discovery of a cool planet of 5.5 Earth masses through gravitational microlensing. Nature, 439:437–440, January 2006. doi: 10.1038/nature04441.

K. Beuermann, S. Dreizler, F. V. Hessman, and J. Deller. The quest for companions to post-common envelope binaries. III. A reexamination of <ASTROBJ>HW Virginis</ASTROBJ>. A&A, 543:A138, July 2012. doi: 10.1051/0004-6361/201219391.

A. Bhattacharya, J. P. Beaulieu, D. P. Bennett, J. Anderson, N. Koshimoto, J. R. Lu, V. Batista, J. W. Blackman, I. A. Bond, A. Fukui, C. B. Henderson, Y. Hirao, J. B. Marquette, P. Mroz, C. Ranc, and A. Udalski. WFIRST Exoplanet Mass Measurement Method Finds a Planetary Mass of 39 ± 8 Earth masses for OGLE-2012-BLG-0950Lb. *ArXiv e-prints*, art. arXiv:1809.02654, September 2018.

Ö. Çakirli and A. Devlen. UBVR photometry of pre-catacylismic binaries: HW Virginis. A&AS, 136:27–33, April 1999. doi: 10.1051/aas:1999196.

D. J. Carnochan and R. Wilson. A survey of ultraviolet objects. MNRAS, 202:317–345, January 1983. doi: 10.1093/mnras/202.2.317.

J. E. Chambers. A hybrid symplectic integrator that permits close encounters between massive bodies. MNRAS, 304:793–799, April 1999. doi: 10.1046/j.1365-8711.1999.02379.x.

P. Charbonneau. Genetic Algorithms in Astronomy and Astrophysics. *The Astrophysical Journal Supplement Series*, 101:309, December 1995. doi: 10.1086/192242.

A. Cheetham, D. Ségransan, S. Peretti, J.-B. Delisle, J. Hagelberg, J. Beuzit, T. Forveille, M. Marmier, S. Udry, and F. Wildi. Direct imaging of an ultracool substellar companion to the exoplanet host star HD 4113A. *ArXiv e-prints*, December 2017.

J. Eastman, R. Siverd, and B. S. Gaudi. Achieving Better Than 1 Minute Accuracy in the Heliocentric and Barycentric Julian Dates. PASP, 122:935, August 2010. doi: 10.1086/655938.

Mahmoud Fouz, Manfred Kufleitner, Bodo Manthey, and Nima Zeini Jahromi. On Smoothed Analysis of Quicksort and Hoare's Find. *ArXiv e-prints*, art. arXiv:0904.3898, April 2009.

B. S. Gaudi. Microlensing Surveys for Exoplanets. ARA&A, 50:411–453, September 2012. doi: 10.1146/annurev-astro-081811-125518.

Z. Han, P. Podsiadlowski, P. F. L. Maxted, T. R. Marsh, and N. Ivanova. The origin of subdwarf B stars - I. The formation channels. MNRAS, 336:449–466, October 2002. doi: 10.1046/j.1365-8711.2002.05752.x.

U. Heber. Hot Subluminous Stars. PASP, 128(8):082001, August 2016. doi: 10.1088/1538-3873/128/966/082001.

J. Horner, T. C. Hinse, R. A. Wittenmyer, J. P. Marshall, and C. G. Tinney. A dynamical analysis of the proposed circumbinary HW Virginis planetary system. MNRAS, 427:2812–2823, December 2012. doi: 10.1111/j.1365-2966.2012.22046.x.

I. D. Howarth. On stellar limb darkening and exoplanetary transits. MNRAS, 418:1165–1175, December 2011. doi: 10.1111/j.1365-2966.2011.19568.x.

C. İbanoğlu, Ö. Çakırlı, G. Taş, and S. Evren. High-speed photometry of the pre-cataclysmic binary HW Virginis and its orbital period change. A&A, 414:1043–1048, February 2004. doi: 10.1051/0004-6361:20034013.

John B. Irwin. The Determination of a Light-Time Orbit. ApJ, 116:211, July 1952. doi: 10.1086/145604.

D. Kilkenny, F. Marang, and J. W. Menzies. A Period Decrease in the Sdb Eclipsing Binary System Hw-Virginis. MNRAS, 267:535, April 1994. doi: 10.1093/mnras/267.3.535.

D. Kilkenny, S. Keuris, F. Marang, G. Roberts, F. van Wyk, and W. Ogloza. On the orbital periods of three close binaries with hot subdwarf primaries. *The Observatory*, 120:48–59, February 2000.

D. Kilkenny, F. van Wyk, and F. Marang. The sdB eclipsing system HW Vir: a substellar companion? *The Observatory*, 123:31–36, February 2003.

L. L. Kiss, B. Csák, K. Szatmáry, G. Furész, and K. Sziládi. Spectrophotometry and period analysis of the sdB eclipsing binary HW Virginis. A&A, 364:199–204, December 2000.

J. W. Lee, S.-L. Kim, C.-H. Kim, R. H. Koch, C.-U. Lee, H.-I. Kim, and J.-H. Park. The sdB+M Eclipsing System HW Virginis and its Circumbinary Planets. AJ, 137:3181–3190, February 2009. doi: 10.1088/0004-6256/137/2/3181.

A.-L. Maire, A. J. Skemer, P. M. Hinz, S. Desidera, S. Esposito, R. Gratton, F. Marzari, M. F. Skrutskie, B. A. Biller, D. Defrère, V. P. Bailey, J. M. Leisenring, D. Apai, M. Bonnefoy, W. Brandner, E. Buenzli, R. U. Claudi, L. M. Close, J. R. Crepp, R. J. De Rosa, J. A. Eisner, J. J. Fortney, T. Henning, K.-H. Hofmann, T. G. Kopytova, J. R. Males, D. Mesa, K. M. Morzinski, A. Oza, J. Patience, E. Pinna, A. Rajan, D. Schertl, J. E. Schlieder, K. Y. L. Su, A. Vaz, K. Ward-Duong, G. Weigelt, and C. E. Woodward. The LEECH Exoplanet Imaging Survey. Further constraints on the planet architecture of the HR 8799 system. A&A, 576: A133, April 2015. doi: 10.1051/0004-6361/201425185.

C. Marois, B. Zuckerman, Q. M. Konopacky, B. Macintosh, and T. Barman. Images of a fourth planet orbiting HR 8799. Nature, 468:1080–1083, December 2010. doi: 10.1038/nature09684.

M. Mayor, D. Queloz, G. Marcy, P. Butler, R. Noyes, S. Korzennik, M. Krockenberger, P. Nisenson, T. Brown, T. Kennelly, C. Rowland, S. Horner, G. Burki, M. Burnet, and M. Kunzli. 51 Pegasi. IAU Circ., 6251, October 1995.

J. W. Menzies and F. Marang. A New B-Subdwarf Eclipsing Binary with an Extremely Short Period. In J. B. Hearnshaw and P. L. Cottrell, editors, *Instrumentation and Research Programmes for Small Telescopes*, volume 118 of *IAU Symposium*, page 305, 1986.

V. Nascimbeni, G. Piotto, L. R. Bedin, and M. Damasso. TASTE: The Asiago Search for Transit timing variations of Exoplanets. I. Overview and improved parameters for HAT-P-3b and HAT-P-14b. A&A, 527:A85, March 2011. doi: 10.1051/0004-6361/201015199.

V. Nascimbeni, A. Cunial, S. Murabito, P. V. Sada, A. Aparicio, G. Piotto, L. R. Bedin, A. P. Milone, A. Rosenberg, A. Zurlo, L. Borsato, M. Damasso, V. Granata, and L. Malavolta. TASTE. III. A homogeneous study of transit time variations in WASP-3b. A&A, 549:A30, January 2013. doi: 10.1051/0004-6361/201219601.

F. H. Navarrete, D. R. G. Schleicher, J. Zamponi, and M. Völschow. The Applegate mechanism in Post-Common-Envelope Binaries: Investigating the role of rotation. *ArXiv e-prints*, March 2018.

F. Pepe, C. Lovis, D. Ségransan, W. Benz, F. Bouchy, X. Dumusque, M. Mayor, D. Queloz, N. C. Santos, and S. Udry. The HARPS search for Earth-like planets in the habitable zone. I. Very low-mass planets around <ASTROBJ>HD 20794</ASTROBJ>, <ASTROBJ>HD 85512</ASTROBJ>, and <ASTROBJ>HD 192310</ASTROBJ>. A&A, 534:A58, October 2011. doi: 10.1051/0004-6361/201117055.

M. Perryman, J. Hartman, G. Á. Bakos, and L. Lindegren. Astrometric Exoplanet Detection with Gaia. ApJ, 797:14, December 2014. doi: 10.1088/0004-637X/797/1/14.

G. Pietrzyński, D. Graczyk, W. Gieren, I. B. Thompson, B. Pilecki, A. Udalski, I. Soszyński, S. Kozłowski, P. Konorski, K. Suchomska, G. Bono, P. G. P. Moroni, S. Villanova, N. Nardetto, F. Bresolin, R. P. Kudritzki, J. Storm, A. Gallenne, R. Smolec, D. Minniti, M. Kubiak, M. K. Szymański, R. Poleski, Ł. Wyrzykowski, K. Ulaczyk, P. Pietrukowicz, M. Górski, and P. Karczmarek. An eclipsing-binary distance to the Large Magellanic Cloud accurate to two per cent. Nature, 495:76–79, March 2013. doi: 10.1038/nature11878.

D. L. Pollacco, I. Skillen, A. Collier Cameron, D. J. Christian, C. Hellier, J. Irwin, T. A. Lister, R. A. Street, R. G. West, D. R. Anderson, W. I. Clarkson, H. Deeg, B. Enoch, A. Evans, A. Fitzsimmons, C. A. Haswell, S. Hodgkin, K. Horne, S. R. Kane, F. P. Keenan, P. F. L. Maxted, A. J. Norton, J. Osborne, N. R. Parley, R. S. I. Ryans, B. Smalley, P. J. Wheatley, and D. M. Wilson. The WASP Project and the SuperWASP Cameras. PASP, 118:1407–1418, October 2006. doi: 10.1086/508556.

S.-B. Qian, L.-Y. Zhu, Z.-B. Dai, E. Fernández-Lajús, F.-Y. Xiang, and J.-J. He. Circumbinary Planets Orbiting the Rapidly Pulsating Subdwarf B-type Binary NY Vir. ApJ, 745:L23, February 2012. doi: 10.1088/2041-8205/745/2/L23.

J. Rameau, G. Chauvin, A.-M. Lagrange, A. Boccaletti, S. P. Quanz, M. Bonnefoy, J. H. Girard, P. Delorme, S. Desidera, H. Klahr, C. Mordasini, C. Dumas, and M. Bonavita. Discovery of a Probable 4-5 Jupiter-mass Exoplanet to HD 95086 by Direct Imaging. ApJ, 772:L15, August 2013. doi: 10.1088/2041-8205/772/2/L15.

D. Ricci, F. G. Ramón-Fox, C. Ayala-Loera, R. Michel, S. Navarro-Meza, L. Fox-Machado, M. Reyes-Ruiz, S. Brown Sevilla, and S. Curiel. Multifilter Transit Observations of WASP-39b and WASP-43b with Three San Pedro Mártir Telescopes. PASP, 127:143, February 2015. doi: 10.1086/680233.

L. Rogers. *It's ONLY Rocket Science: An Introduction in Plain English*. Astronomers' Universe. Springer, 2008. ISBN 9780387753775. URL https://books.google.it/books?id=75b84eC-ulsC.

G. Scandariato, D. Ehrenreich, I. Pagano, D. Queloz, Y. Alibert, R. Alonso, T. Bárczy, W. Baumjohann, W. Benz, X. Bonfils, A. Brandeker, L. Borsato, C. Broeg, J. Cabrera, S. Charnoz, A. C. Cameron, M. Davies, O. Demangeon, M. Deleuil, A. Erikson, A. Fortier, L. Fossati, M. Fridlund, D. Gandolfi, M. Gillon, M. Güdel, K. Isaak, L. Kiss, J. Laskar, C. Lovis, M. R. Meyer, V. Nascimbeni, G. Oloffson, E. Pallé, G. Piotto, D. Pollacco, R. Ragazzoni, N. Rando, É. Renottes, I. Ribas, N. C. Santos, S. Sousa, T. Spohnl, M. Steller, G. Szabó, N. Thomas, S. Udry, N. Walton, D. Barrado y Novascués, A. Gutierrez Peña, A. Lecavelier des Etangs, and V. Van Grootel. CHEOPS (Characterising Exoplanets Satellite) Mission. In *Frontier Research in Astrophysics II*, page 89, May 2016.

D. R. G. Schleicher and R. E. Mennickent. A dynamo mechanism as the potential origin of the long cycle in double periodic variables. A&A, 602:A109, June 2017. doi: 10.1051/0004-6361/201628900.

R. A. Smullen, K. M. Kratter, and A. Shannon. Planet scattering around binaries: ejections, not collisions. MNRAS, 461:1288–1301, September 2016. doi: 10.1093/mnras/stw1347.

J. Southworth. Homogeneous studies of transiting extrasolar planets - I. Light-curve analyses. MNRAS, 386:1644–1666, May 2008. doi: 10.1111/j.1365-2966.2008.13145.x.

J. Southworth. JKTEBOP: Analyzing light curves of detached eclipsing binaries. Astrophysics Source Code Library, July 2012a.

J. Southworth. Eclipsing Binary Stars: the Royal Road to Stellar Astrophysics. In F. Arenou and D. Hestroffer, editors, *Orbital Couples: Pas de Deux in the Solar System and the Milky Way*, pages 51–58, May 2012b.

M. Völschow, D. R. G. Schleicher, V. Perdelwitz, and R. Banerjee. Eclipsing time variations in close binary systems: Planetary hypothesis vs. Applegate mechanism. A&A, 587:A34, March 2016. doi: 10.1051/0004-6361/201527333.

M. Völschow, D. R. G. Schleicher, R. Banerjee, and J. H. M. M. Schmitt. The physics of the Applegate mechanism: Eclipsing time variations from magnetic activity. *ArXiv e-prints*, September 2018.

Peter J. Wheatley, Richard G. West, Michael R. Goad, James S. Jenkins, Don L. Pollacco, Didier Queloz, Heike Rauer, Stéphane Udry, Christopher A. Watson, Bruno Chazelas, Philipp Eigmüller, Gregory Lambert, Ludovic Genolet, James McCormac, Simon Walker, David J. Armstrong, Daniel Bayliss, Joao Bento, François Bouchy, Matthew R. Burleigh, Juan Cabrera, Sarah L. Casewell, Alexander Chaushev, Paul Chote, Szilárd Csizmadia, Anders Erikson, Francesca Faedi, Emma Foxell, Boris T. Gänsicke, Edward Gillen, Andrew Grange, Maximilian N. Günther, Simon T. Hodgkin, James Jackman, Andrés Jordán, Tom Louden, Lionel Metrailler, Maximiliano Moyano, Louise D. Nielsen, Hugh P. Osborn, Katja Poppenhaeger, Roberto Raddi, Liam Raynard, Alexis M. S. Smith, Maritza Soto, and Ruth Titz-Weider. The Next Generation Transit Survey (NGTS). MNRAS, 475:4476–4493, April 2018. doi: 10.1093/mnras/stx2836.

Kevin Williams and Michael Guidry. Application of Genetic Algorithms to a variety of problems in Physics and Astronomy. In *APS Southeastern Section Meeting Abstracts*, volume 71, page DD.005, November 2004.

A. Wolszczan and D. A. Frail. A planetary system around the millisecond pulsar PSR1257 + 12. Nature, 355:145–147, January 1992. doi: 10.1038/355145a0.

J. H. Wood and R. Saffer. Spectroscopy of the post-common envelope binary HW Virginis. MNRAS, 305:820–828, May 1999. doi: 10.1046/j.1365-8711.1999.02501.x.

J. H. Wood, E.-H. Zhang, and E. L. Robinson. HW Virginis - A short period eclipsing binary containing an sdB star. MNRAS, 261:103–112, March 1993. doi: 10.1093/mnras/261.1.103.